Navy Department
Bureau of Ordnance
Contract NOrd 9612

Preliminary Report on

THE EFFECT OF JETS ON THE DRAG AND CAVITATION CHARACTERISTICS OF A TWO-DIMENSIONAL BODY

By

J.T. McGraw, R.W. Kermeen, V.G. Jackson

Hydrodynamics Laboratories
California Institute of Technology
Pasadena, California

Memorandum Report No. EM-12
July 2, 1951

J. T. McGraw
Project Supervisor

Copy No. 109

CONTENTS

ABSTRACT

The effect of hydrojets on the drag characteristics of a two-dimensional hydrofoil was investigated in the High Speed Water Tunnel. The jets were found to affect drag through changes both in skin friction and pressure distribution, and when cavitating they showed some additional change.

INTRODUCTION

The development of hydrojet powered torpedoes has presented a new group of hydrodynamic problems for the designer. Among the items of interest are the effects of the hydrojets on the drag and cavitation performance of the body.

There are two radically different schemes in the pump and jet arrangement for bodies of revolution. (a) A single entrance to the pump at the bow leading to the outlet on the forward part of the missile; (b) entrance near the after part leading to a single discharge at the stern of the body. The Mk 40 is of type (a), having a discharge of eight jets, and this research is directed toward facilitating the solution of problems arising from this configuration, and does not consider any of the problems of type (b).

The Mk 40 test vehicle was subjected to model drag tests at Stevens Institute of Technology and at this Laboratory. The results of the two laboratories showed enough disagreement to establish the need for further work. The presence of shields and the complications caused by the numerous jets made the accurate experimental determination difficult.

To develop a more fundamental attack on the problem, a series of conferences was held with a representative from the Naval Ordnance Test Station, Pasadena, and a research program was outlined. It was decided that it would be most valuable to determine the effect of hydrojets on the magnitude of the drag and to determine the mechanism by which the hydrojets increased the drag. To start with the simplest case, a two-dimensional hydrofoil with two symmetrical jets was selected as the test vehicle since with this shape the support interferences and experimental difficulties could be reduced to a minimum. It was not expected that the results could be applied directly to bodies of revolution, but it was hoped that an accurate experimental investigation and analysis of the specific case would lead to a better understanding of the problem.

PURPOSE

The purpose of the investigation was to determine the magnitude of the drag increment due to water jets emerging from a two-dimensional body and to study the hydrodynamic causes for the change in drag.

CONCLUSIONS

1. For the hydrofoil model tested, the hydrojets decrease the drag at low jet velocities and then increase it as the jet velocities are increased.

2. At higher Reynolds numbers (based on chord length and tunnel velocity) the drag increases with U/V, the jet-to-tunnel velocity ratio.

3. At the highest Reynolds numbers and constant U/V the curve of drag coefficient (based on plan area) as a function of Reynolds number approaches the same slope as that for turbulent skin friction for flat plates.

4. The maximum drag reduction at U/V less than 1 is approximately equal to the drag increase due to the presence of the inoperative jet nozzles in the model surface.

5. The mechanism by which the jets affect the drag characteristics is both through increased skin friction and changes in pressure distribution.

6. The jets cause a more efficient pressure recovery over the afterbody along the axis of the jets.

7. The local low pressure region immediately behind the jet nozzle makes the body more susceptible to cavitation than the bare body, particularly at high U/V.

8. At constant flow rate jet cavitation increases the thrust and also the drag, but to a lesser degree.

APPARATUS

The two-dimensional brass model used in these tests was an NACA 63-010 hydrofoil* with a 7.5-in. chord, modified by shortening the trailing edge 3/16 in. This was necessary because of the machining difficulties with the thin trailing edge of the full length model. This hydrofoil provided a convenient thickness ratio for attaching the balance spindle and drilling the internal jet passages, and in addition this section has a pressure profile similar in shape though with lower pressures than that of the Lyon's form A** which was used for the Mk 40 torpedo.

A force section with a 2-in. span, Fig. 1, was chosen instead of one with a full span across the working section primarily because of the geometry of the balance in the High Speed Water Tunnel. This balance, which is of the NPL type, consists of a spindle or lever hinged in the middle with the model attached at the upper end and the forces measured at the lower end by means of hydraulic cylinders. Thus the drag is measured as a moment and is not separated from pitching moment. Any lack of symmetry in the model or stream pattern would result in greater errors in drag readings when integrated across a wide span. However, it was necessary to have a span wide enough to insure that the jets in mixing with the stream do not spread beyond the edges of the force section, that the flow is uniform across this section, and that the edge or gap effects are small compared with the forces to be investigated. In addition, the 2-in. span gave a ratio of surface area to jet cross sectional area approximately the same as that of the Mk 40 test vehicle. Two 6-in span sections fastened to the working section walls were used for spindle shields and to complete the span, Fig. 2.

The jets consist of two symmetrically located holes in the surface which intersect the plane of symmetry of the section at an angle of 12 degrees. The jet nozzles are of the flush type made by drilling holes 0.153 in. in diameter giving the water an average straight path of 1.625 in. before the jet exit on the surface of the hydrofoil. The axis of the jets intersects the surface at 30% chord point of the unshortened hydrofoil, which is also the point of lowest pressure. The spindle is attached at the 35% chord point

---

*NACA Report No. 824, "Summary of Airfoil Data", 1945.

**Lyon, Hilda M., "Effect of Turbulence on Drag of Airship Models", 1932.

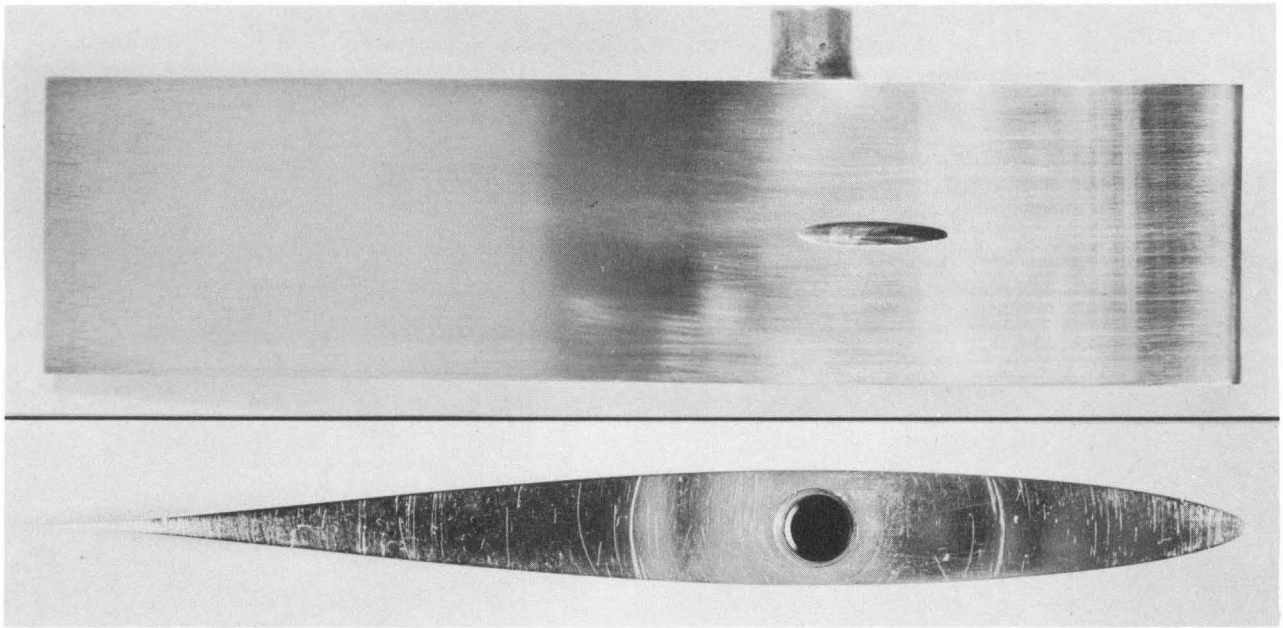

Fig. 1 - NACA 63-010 jet hydrofoil force section, chord 7-5/16 in.; span 2 in.

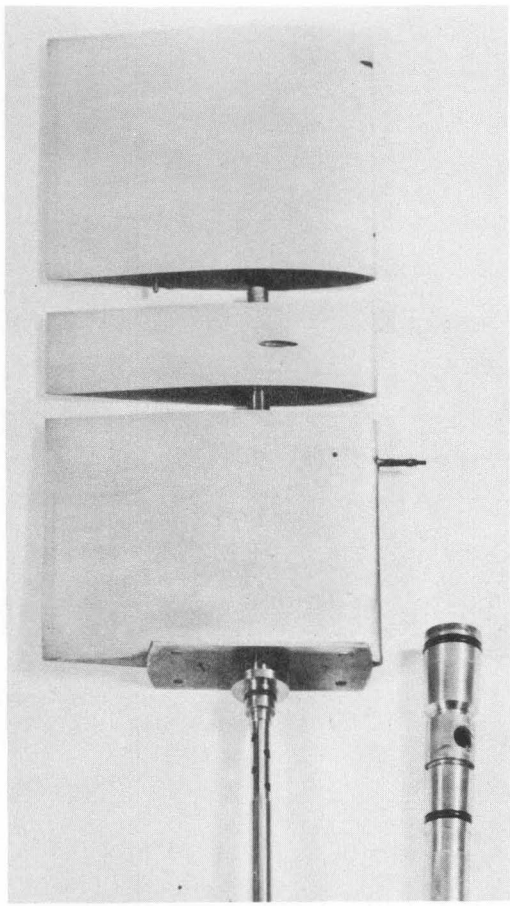

Fig. 2 - Hydrofoil model showing span section (upper), force section (center) spindle shield (lower), and hollow spindle (lower right)

where the hydrofoil has a maximum thickness of 0.750 in. For symmetry a short cylinder 1/2 in. long extends into the upper shield from the force section to simulate the spindle which extends from the lower shield to the force section. The turbulence in the jets, due to the roughness of passages inside the force section and the nature of the flush jet nozzles, causes the jets to break up somewhat into a spray rather than to discharge as smooth jets, Fig. 3. The spread of the jets varies with velocity.

A pressure distribution section of the jet hydrofoil with 42 pressure taps, Fig. 4, was used to determine the effects of the jets on the pressure field around the model. The pressure taps are holes 0.030 in. in diameter, drilled perpendicular to the surface. The taps were arranged in three rows behind the jet nozzles to show spanwise variation in the pressure behind the jet. One row of pressure taps was located on the axis of the jets, one 1/8 in. above and the other 1/2 in. above this axis. Fig. 5 shows the pressure distribution section installed in the tunnel.

Water for the jets was removed from a remote portion of the tunnel approximately 150 ft upstream from the working section and pumped to the model by a turbine type pump driven by a 5-hp. motor, Fig. 6. At maximum capacity the pump delivered 0.0154 cu. ft per sec to the model at 275 psi. For photographic studies of the jets a saturated solution of potassium permanganate was injected into the stream at the pump inlet.

The problem of supplying high velocity water to the model without affecting the force measurements was solved by introducing it at the hinge point of the spindle as shown in Fig. 7 and the sketch, Fig. 8. The force section was mounted on a hollow spindle which was supported in the existing balance frame by wire supports. By introducing the water at the hinge point of the balance and normal to the tunnel axis, any direct force applied at this point would not affect the force measurements and only a moment in the plane of the hydrofoil would affect the drag. A three-turn coil of 5/8 in. copper tubing was used for the spindle water connection. Any tendency of the coil to unwrap can only affect the cross force, and any moment about the spindle axis is read as yawing moment. Flexible hose pump-to-spindle connections were tried first but the pressure developed to the lines at maximum jet velocity was 275 psig, which caused the hoses to stiffen and introduced tares of the same order as the forces being measured. The coil of tubing was

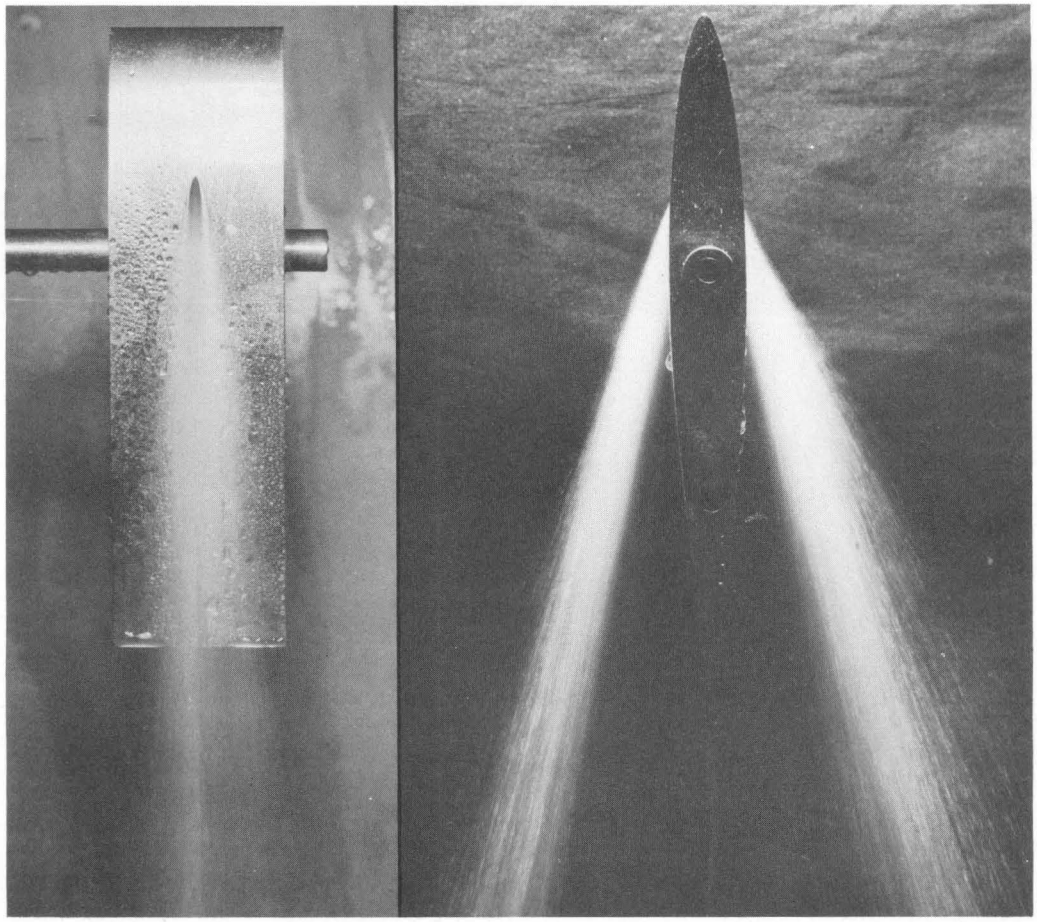

U = 50 fps U = 100 fps

Fig. 3 - Breakup of jets in air

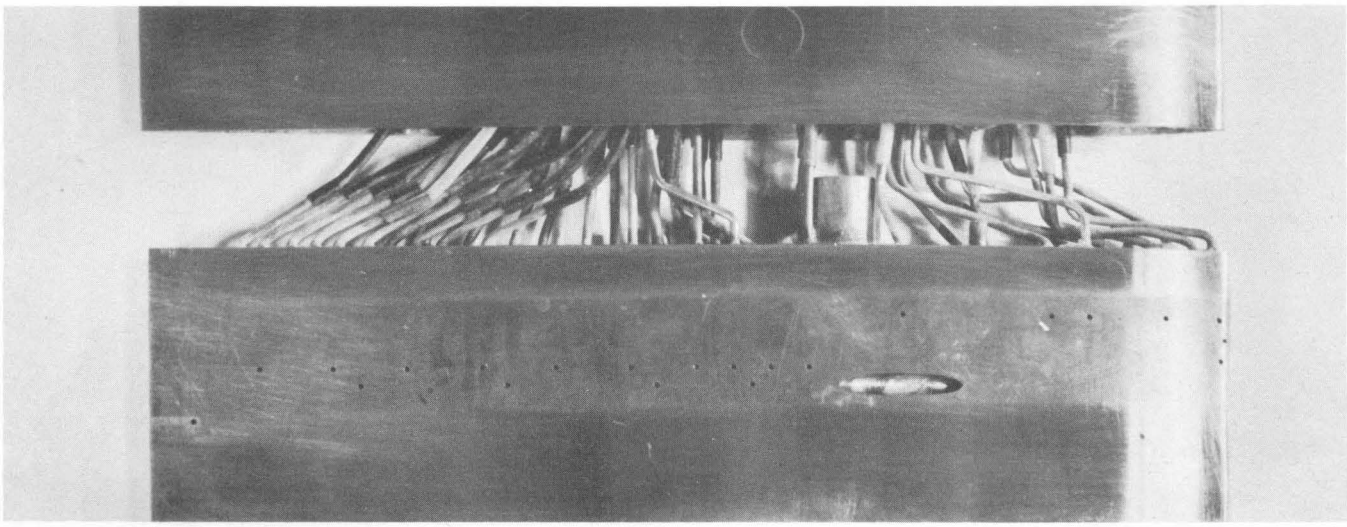

Fig. 4 - Pressure distribution section showing the pressure taps and the tubing connections in the upper shield

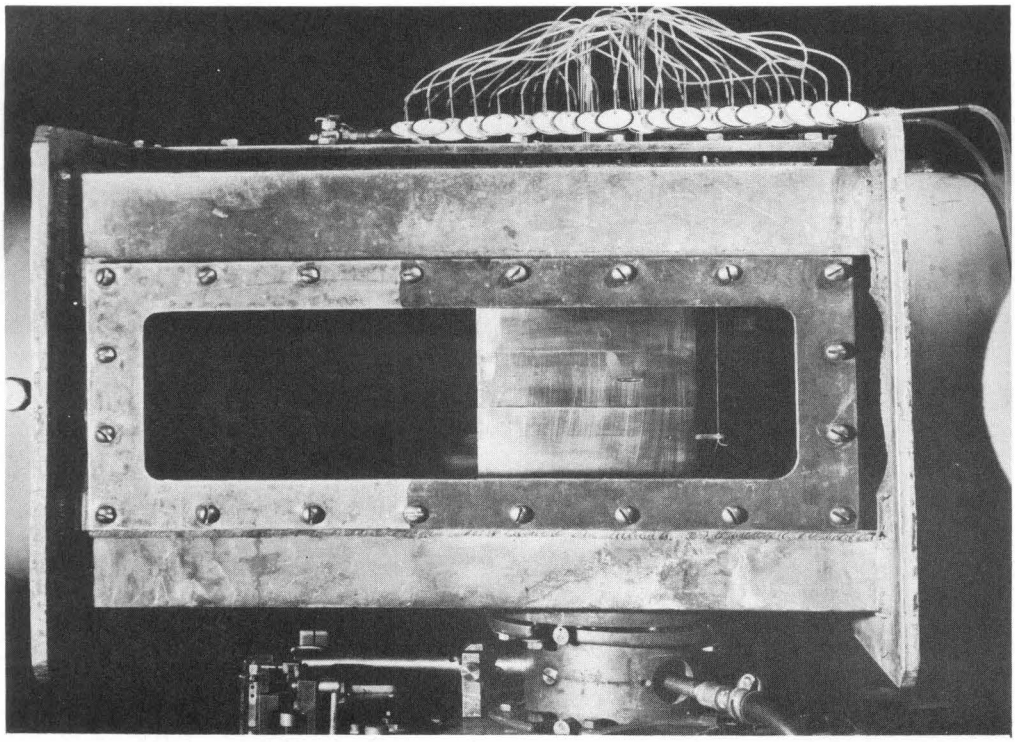

Fig. 5 - Setup in the working section for pressure distribution measurements

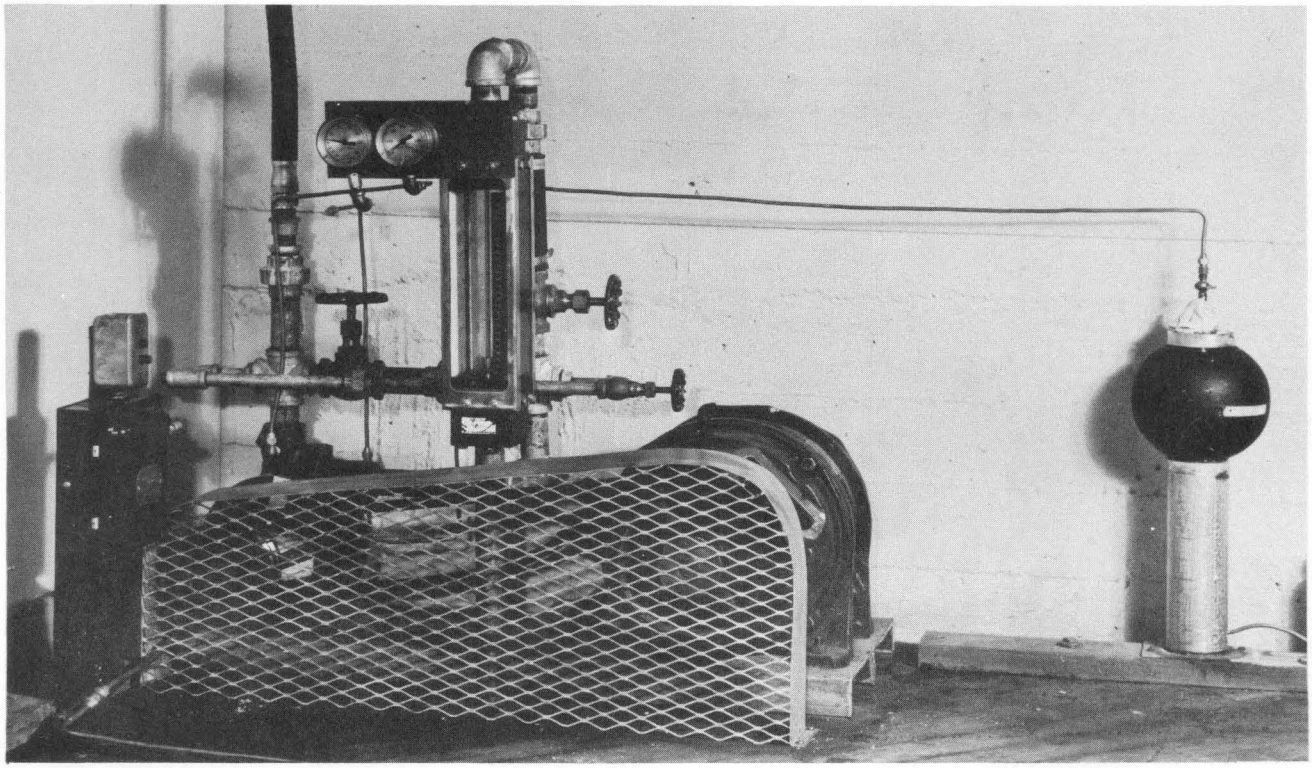

Fig. 6 - Pump for supplying water to model. Note rotameter

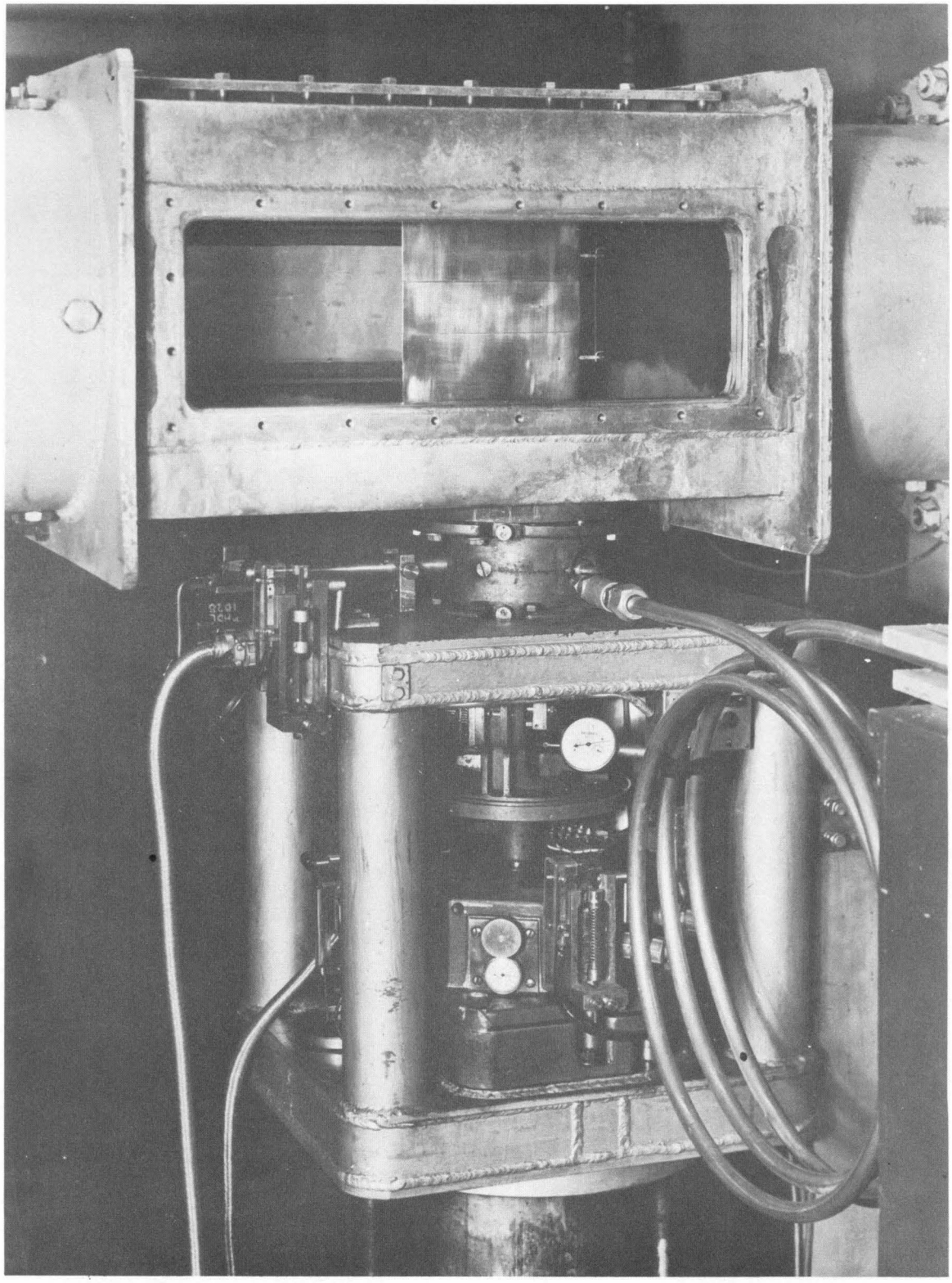

Fig. 7 - Jet hydrofoil mounted on balance with the jet water supply coil attached to the spindle

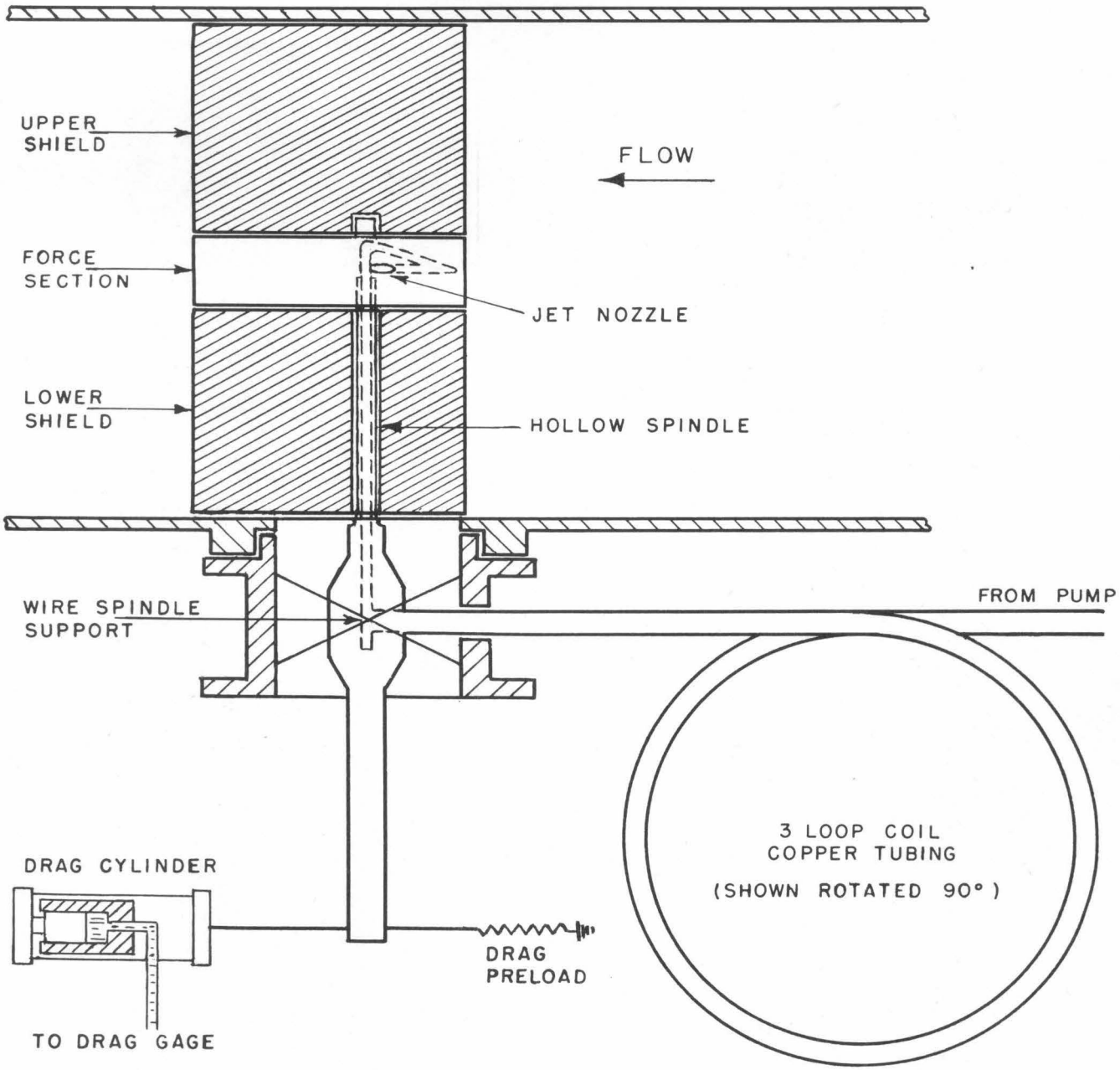

Fig. 8 - Jet hydrofoil and balance schematic showing water connection at the hinge point of the spindle

substituted and remained flexible at all pressures. The measurements were not affected by small movements of the spindle. The coil of tubing served somewhat to damp out the vibrations from the model water supply pump and since the same setup was used in both thrust and drag measurements, any small tares involved are subtracted out with the thrust forces.

PROCEDURE

Before force and pressure distribution measurements could be made, it was necessary to investigate all extraneous factors suspected of influencing the results, such as forces caused by the spindle water connection, boundary layer conditions, drag on the model support spindle, the effect of shield gaps, and the thrust characteristics of the jets themselves. The results of these preliminary investigations are reported in the appendix.

Some of the terms used in this report are defined below:

Thrust is the measured reaction with the jets discharging into air. The thrust in these experiments varied in the discharge pressure due to cavitation. Pressures at the jet outlets for various tunnel conditions were calculated from tunnel pressure and velocity, and the smooth body pressure distribution. Thrust was then assumed to be the same as that measured at the air pressure corresponding to the calculated jet discharge pressure.

The drag due to the jet opening is the difference between the body resistance measured with the jet holes open but without flow, and the resistance measured for the smooth body.

The drag due to the jets is the difference between the body resistance measured with the jets in operation and the resistance measured with the jet holes open but without any flow.

The jet nozzles were sealed and smoothed with wax for the drag and pressure distribution measurements without jets. Other runs were made with the jet nozzles open but with no flow through them.

In order to determine the effect of the jets on drag, it was necessary to measure the combined drag and thrust forces and then to subtract the thrust of the jets. Each run was made at a constant tunnel velocity with the jet velocity varying from 10 to 100 fps. The range of working section velocities was from 10 to 80 fps. The working section velocity was determined in the usual way by measuring the pressure drop across the tunnel nozzle and the

average jet velocities by measuring the volume rate of flow through a Brooks Rotameter at the low pressure side of the model water supply pump, Fig. 6, and dividing by the jet nozzle area.

The data for both the drag and thrust runs were plotted to a large scale and smooth curves were drawn through the points. The appropriate thrust curve was then subtracted from the combined thrust and drag curves to give the drag of the hydrofoil. This method gave more consistent results than a point-to-point method, since the quantities to be subtracted were relatively large numbers. The point method would cause any small scatter in the data to be magnified.

The jets were studied photographically by taking vertical and horizontal pictures simultaneously, thus showing the spread of the jets in two planes. A solution of potassium permanganate was added at the pump to make the jets visible, Fig. 9. The effect of the jets on cavitation was studied in the same manner.

Each pressure distribution run was made at constant U, V, and P_o. The pressures measured were the differences between the working section static pressure at a point on the tunnel wall approximately 11 in. upstream from the model nose and the pressure at each of the 42 taps in the model.

DISCUSSION OF RESULTS

Before attempting to investigate the effect of jet flow upon model drag, it was first necessary to establish the drag characteristics of the basic hydrofoil contour. It was also necessary to determine the effect on drag of the presence of the nozzles in the surface of the hydrofoil. Determination of these reference data thus permitted separation of the influence of the surface discontinuity at the nozzle exit from the influence of the jet flow itself. The presence of the inoperative nozzles was observed to cause a marked increase in the drag of the model. This increase is illustrated by a comparison of the drag coefficients for the model, both with and without jet passages. See Fig. 10.

This measurement of the increase in drag due to the jet holes can be used for predicting drag before or after the jets are operating, and while this is of no significance in predicting the drag caused by jet operation, it serves as the zero point in plotting changes of drag vs. jet velocity.

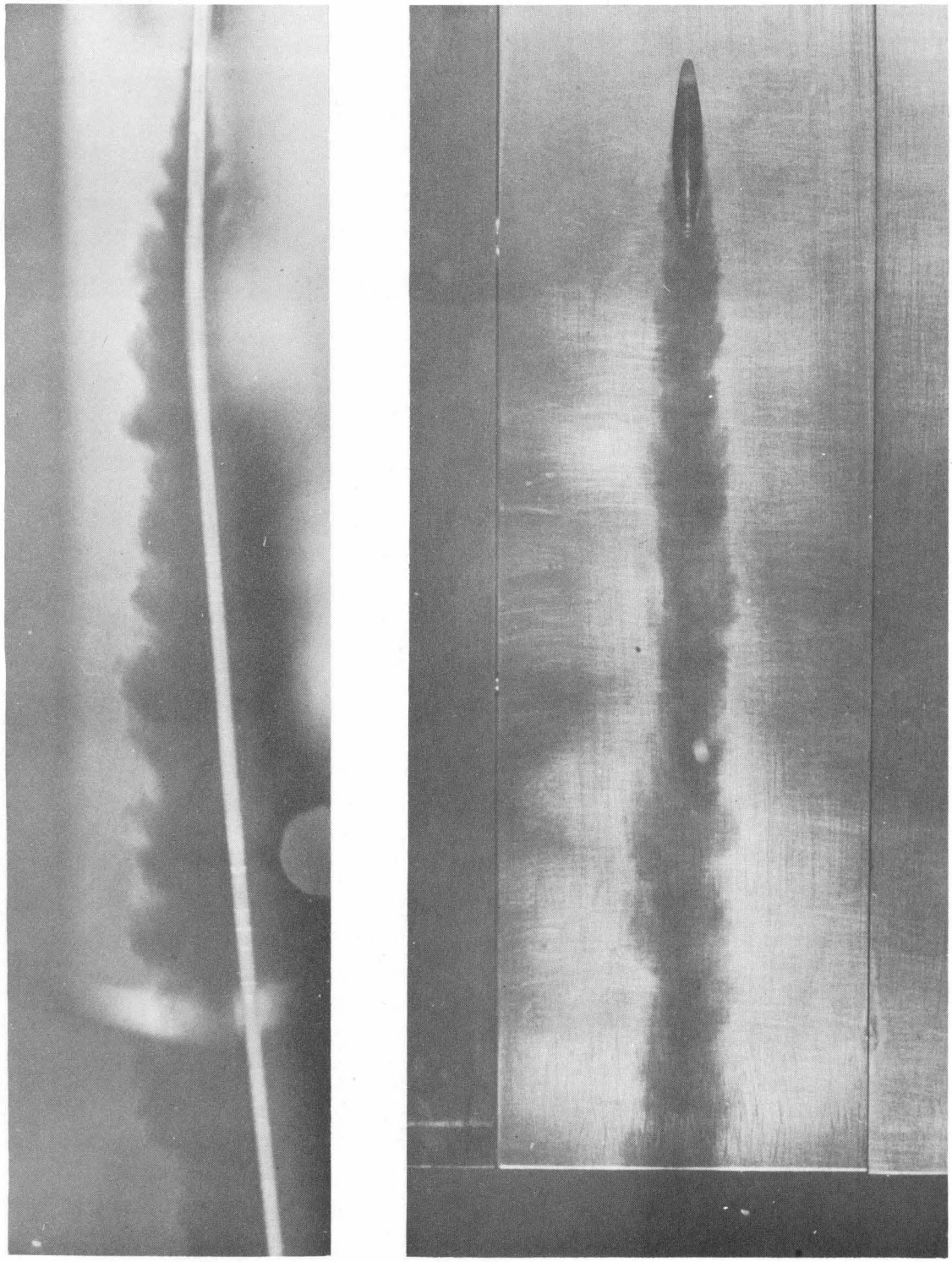

Fig. 9 - Jet profile in vertical and horizontal planes at a jet-to-tunnel velocity ratio of 1.5
Tunnel velocity 60 fps - Jet velocity 90 fps

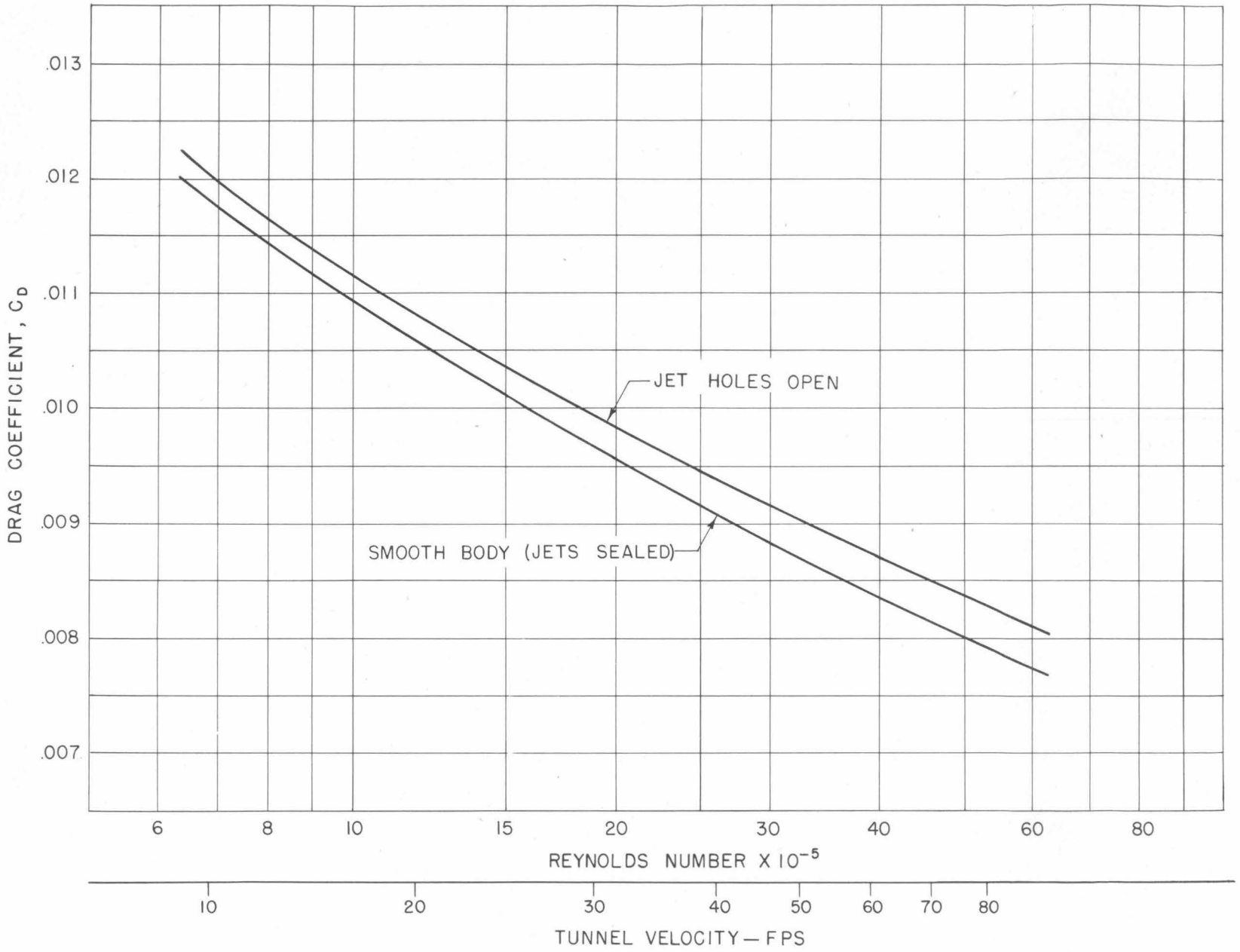

Fig. 10 - Drag coefficient vs. Reynolds number for smooth hydrofoil and with jet nozzles open

CONFIDENTIAL

The drag of the model was then measured with the jets in operation. The range of investigation covered many different combinations of jet velocity and tunnel velocity, with jet velocities varying from 10 to 100 fps and tunnel velocities from 10 to 80 fps. Thrust forces due to the jet flow were measured separately and the balance gage readings adjusted accordingly to indicate the true drag. Information as to experimental procedure and data reduction technique is included in the "Procedure" section. Shown in Fig. 11 are several curves representative of the family of drag curves obtained in this manner. These results show that the jet flow has a small but distinct effect upon the model drag. It can be seen that for any tunnel velocity the change in drag force caused by the jets is small compared to the total drag force on the body. For example, with a jet velocity of 100 fps and a tunnel velocity of 50 fps, i.e., a velocity ratio of 2, the drag was increased by 6.8% Higher velocity ratios lead to greater drag increases. For a velocity ratio of 5, jet velocity 100 fps and tunnel velocity 20 fps, the drag increased 9.0%, but velocity ratios of less than 2 caused drag increases of less than 7.2% in all cases measured.

The magnitude and nature of this change can be observed more clearly if the results are replotted to show only the changes themselves due to the jet flow. That is, the value of the drag coefficient for zero jet velocity is subtracted from the value of the drag coefficient with the jets in operation at various velocities. These reduced data are shown plotted in Fig. 12.

The general effect of jet flow is similar for all tunnel velocities. As the jet velocity increases from zero the drag initially decreases. This trend is reversed by further increases in jet velocity and the model drag ultimately increases to values in excess of the drag with no jet flow. The maximum drag reduction caused by the jet flow is, as a rule, smaller than the drag increase caused by the presence of the nozzle holes in the surface of the hydrofoil and becomes equal to it only when the jet velocity is less than tunnel velocity. This precludes the consideration of these values for use in predicting optimum conditions for a propulsion unit.

A composite picture of the effect of jets on the drag is obtained if curves of drag coefficient vs. Reynolds number for various jet-to-tunnel velocity ratios are plotted, Fig. 13. Most of these curves, compared with the zero jet flow line, have an inflection point and beyond it a maximum. These

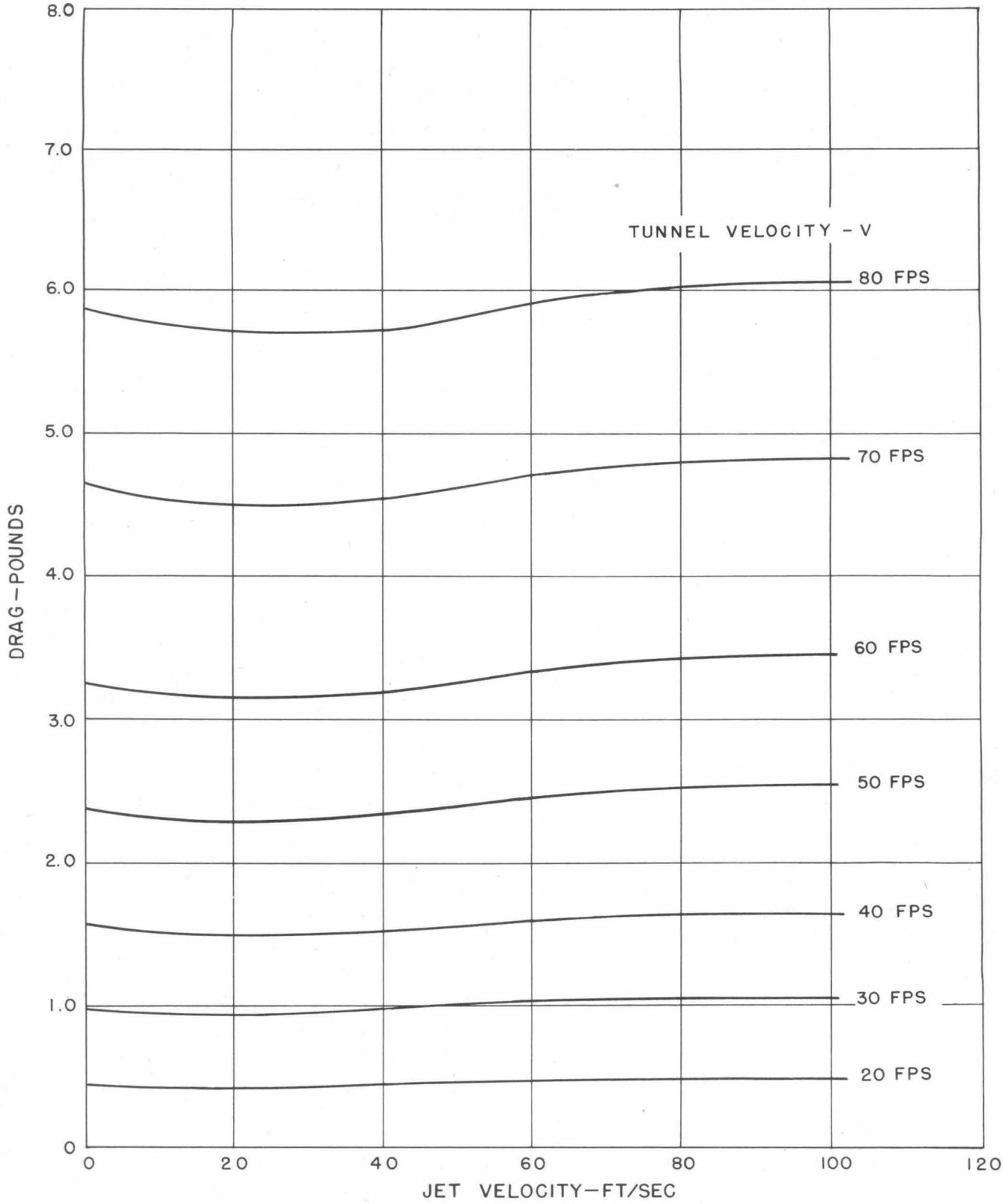

Fig. 11 - Drag vs. jet velocity at various tunnel speeds

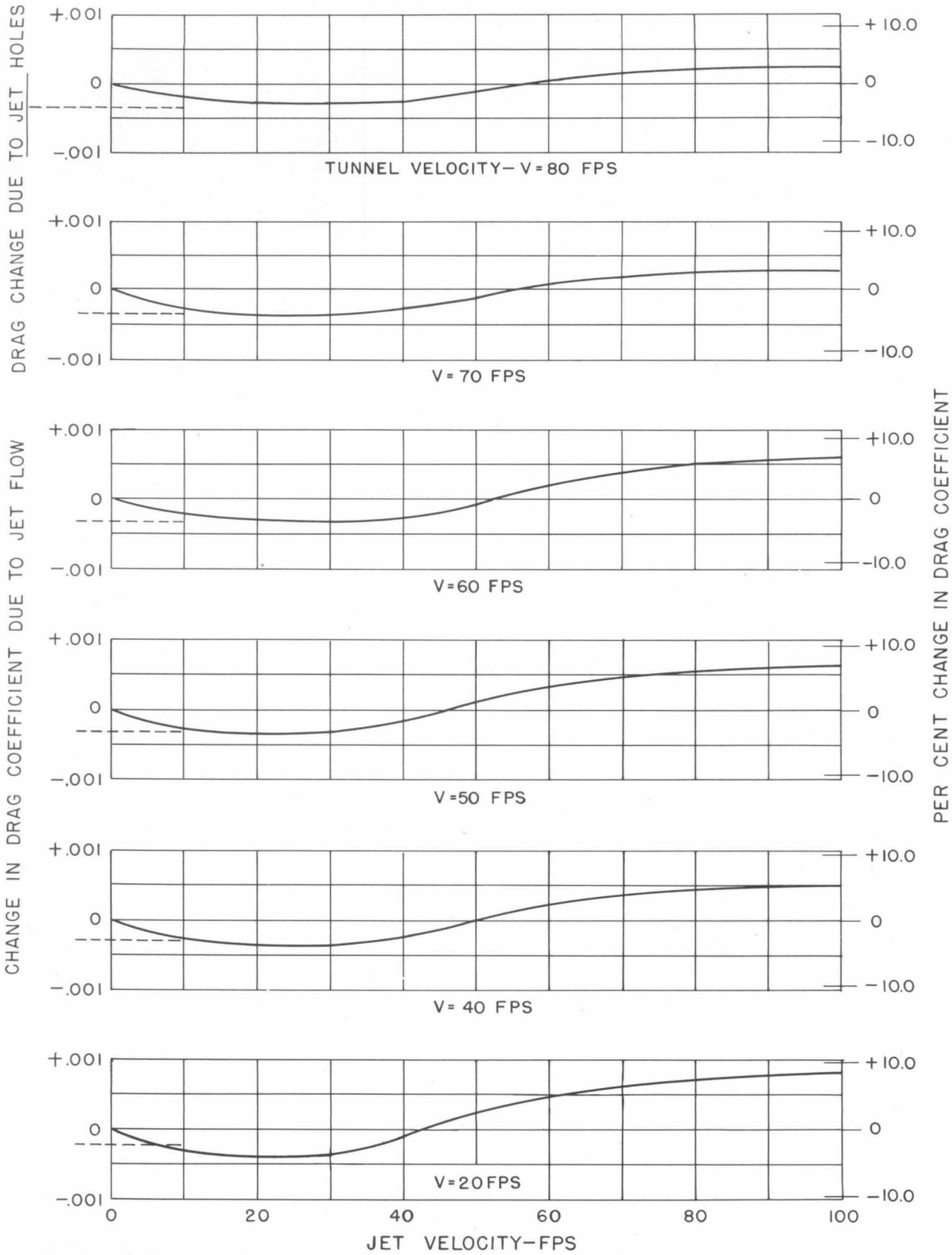

Fig. 12 - Change in drag coefficient vs. jet velocity at various tunnel speeds

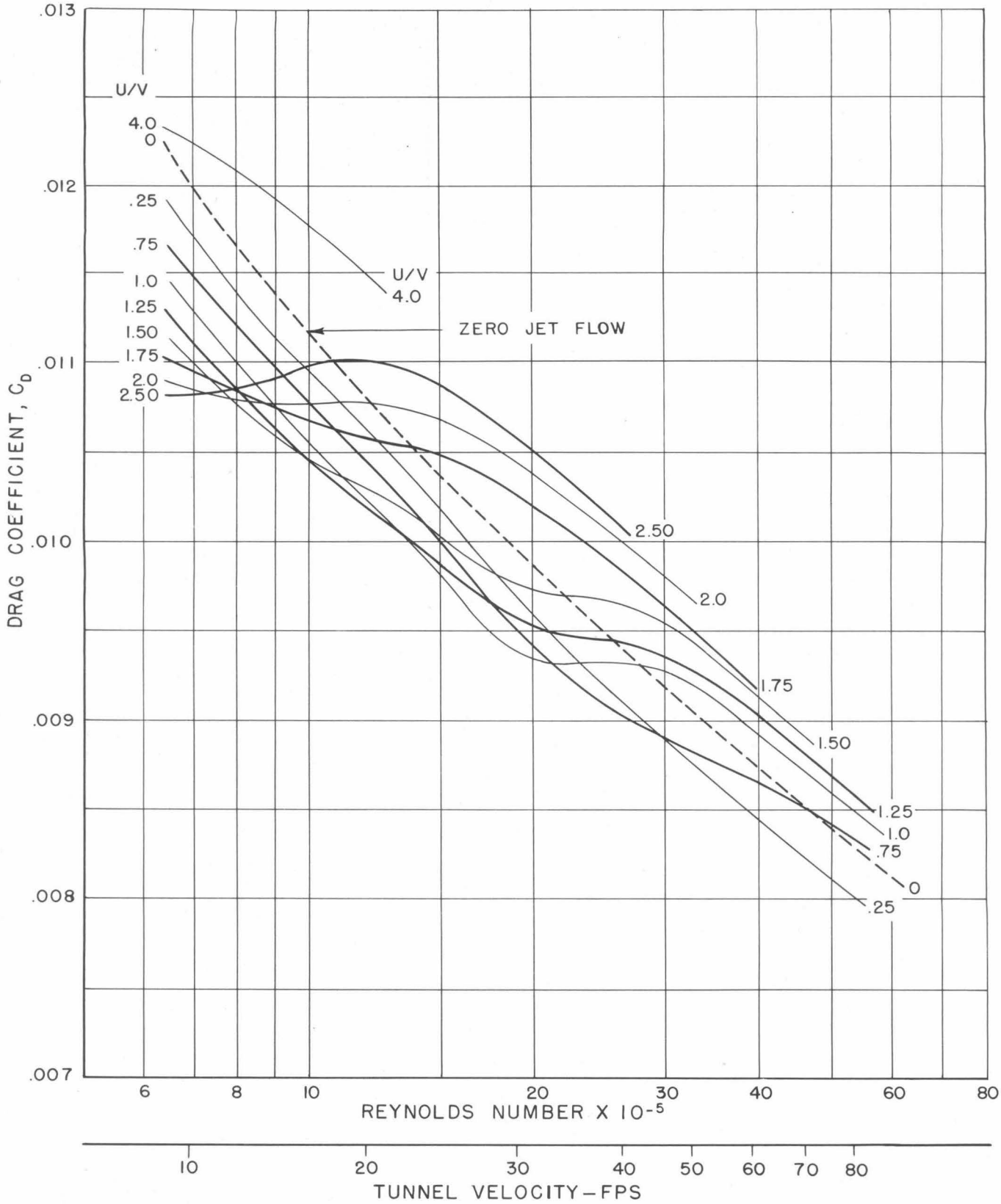

Fig. 13 - Drag coefficient vs. Reynolds number for a series of jet-to-tunnel velocity ratios

maxima occur at lower Reynolds numbers for higher U/V ratios. In the case of U/V ratio of 4 only, the part of the curve beyond the maximum point is within the test range. For U/V = 0.75 the inflection point is still clear, but no maximum develops. Finally at U/V = 0.25 the curve is practically parallel with that for zero jet flow. All drag curves show the tendency to approach the slope of the zero jet flow drag curve at the highest Reynolds numbers and the drag coefficients are there increasing with increased U/V ratio. The only exception is the relative position of the U/V = 0.25 and zero curves. Whether at still higher Reynolds numbers the drag coefficients would all be above the zero jet flow drag coefficient or not, we do not know.

At a Reynolds number 6×10^5 the drag coefficients are decreasing with increasing U/V except for U/V = 4. The reason for this may be, as mentioned above, that the portion of the curve before the maximum is below the test range.

Some of the curves extend over only part of the test range due to the limitations in the present equipment which made it impossible to obtain the higher jet ratios at large Reynolds numbers. It is noted that for U/V = 2.0 the maximum drag increase over the body with open jet passages is 7.2% at a Reynolds number of 30×10^5, and if the lines were parallel with the zero jet flow line, this percentage would increase to 8% at a Reynolds number of 60×10^5. At a velocity ratio of 1.5 the increase is 4.4% at a Reynolds number of 45×10^5, and with equal jet and stream velocities the maximum increase obtained with this model is 3.5% at a Reynolds number of 55×10^5. The maximum increase in drag over the smooth body drag without jet nozzles is 12% at a velocity ratio of 2.0 instead of the 7.2% based on the body with jet holes open but no flow.

The interaction of the jets with the surrounding flow and the model appears to be very complicated and the exact mechanism of the change from drag reduction to drag increase was not determined. The drag reduction is caused by a decrease in profile drag as stated below, and an increase in skin friction resulting from the high velocity jets spreading over a larger area of the body can account for the increased drag. However, the transition between the two occurs at different Reynolds numbers and makes any general statement about the effects of jets on the drag of another model or prototype extremely hazardous.

In order to be able to discuss the mechanism of the effect of jets, it is necessary to separate the profile drag from the skin friction drag. It is to be expected that jet flow will have a marked effect upon the skin friction component of drag. This is due to the scouring action over an area of the hydrofoil by the high velocity jet. Since it was observed that the pressure distribution around the hydrofoil affected the jet flow pattern, see Fig. 14, it was also to be expected that the reverse would be true; the jet flow would have an effect upon the pressure distribution and hence on the profile drag.

From any measured pressure distribution on a model it is generally possible to compute a numerical value for the profile drag in the case of the smooth body without jets. Hence pressure distribution surveys were made for various jet flow conditions using a model shown in Fig. 4. However, with jet flow through the nozzles the pressure distribution around the hydrofoil is no longer two-dimensional because of the three-dimensional character of the expanding jet. Computation of the profile drag thus becomes more difficult, and no quantitative analysis was made to assign any of the measured forces to viscous effects or pressure changes. The region of influence of the jets is very dependent upon the amount of turbulence in the jet and hence the diffusion of the jet after it issues from the nozzles. Fig. 3 shows a photograph of the nozzles discharging into still air, from which it can be seen that the jets diffuse rapidly. Fig. 15 shows the shape of the expanding jet for various velocity ratios. The jet turbulence and rate of diffusion may also affect the pressure field around the model and though no attempt was made to control this factor in the experiment, it should be investigated using various jet nozzle configurations.

Despite the superposition of the three-dimensional jet on the two-dimensional hydrofoil pressure field, it is of interest to observe the trend of the pressure distribution curves for various jet velocities since this will indicate the trend of the profile drag.

The curve, Fig. 16, shows the two-dimensional distribution of pressure coefficient existing around the basic NACA 63-010 hydrofoil without jets. The curves, Fig. 18, taken from measurements of the pressure distribution existing on a line directly behind the jets, are plotted to show only the change caused by the jets in the basic pressure coefficient distribution. The curves for U/V = 7 are shown on both Figs. 16 and 18. On the former is the actual

pressure distribution existing behind the nozzle and on the latter the difference between this and the pressure with sealed nozzles.

It can be seen that the most severely affected region lies directly behind the jet. No changes were observed in the pressure distribution upstream from the jet nozzles. Immediately behind the jet nozzle there is a pressure increase forming a sharp peak which increases with U/V. Slightly farther back, at about the 45% chord point, there is a negative pressure trough with a maximum where the pressure coefficient drops considerably below the smooth body value. This low pressure region is of interest since the local reduction of pressure makes the body more susceptible to cavitation. Fig. 17 shows that except for small amounts of cavitation inside the jet nozzle and at the spindle, this low pressure region began to cavitate first. As a result the cavitation number, K, for incipient cavitation of the model is increased from 0.39 for the basic hydrofoil shape to 0.41 at a jet-to-tunnel velocity ratio of 2.0. At ratios of 3.0 and 7.0 this critical K is 0.44 and 0.73 respectively.

Farther downstream the surface pressure, and hence the pressure coefficient is increased to values above those of the smooth hydrofoil. This increased pressure recovery on the downstream surface of the hydrofoil leads to a reduction of profile drag. Calculations of the profile drag along the axis of the jets, based on the measured pressure distribution, show that in this region beyond the 60% chord point the form drag is considerably reduced. At U/V = 3.5 the profile drag coefficient was reduced 11%, from 0.0045 with zero jet velocity to 0.0040 with 20 fps tunnel velocity.

It had previously been suggested that the only effect of jet flow of this type is to increase the drag by added skin friction caused by the jets against the surface of the body. The data upon which the present report is based do not seem to substantiate this view. The family of curves in Fig. 12 shows a consistent trend in which the presence of jet flow causes a drag reduction for low jet velocities. This behavior can not be explained readily by skin friction considerations alone. Skin friction increases wherever the jet increases the velocity gradient over an area at the model surface, but a concurrent decrease in profile drag may also occur by the action of the jet adding energy to the boundary layer. A resultant increase or decrease in the total drag will depend upon the relative magnitudes of the increase in skin friction drag and the increase or decrease in profile drag.

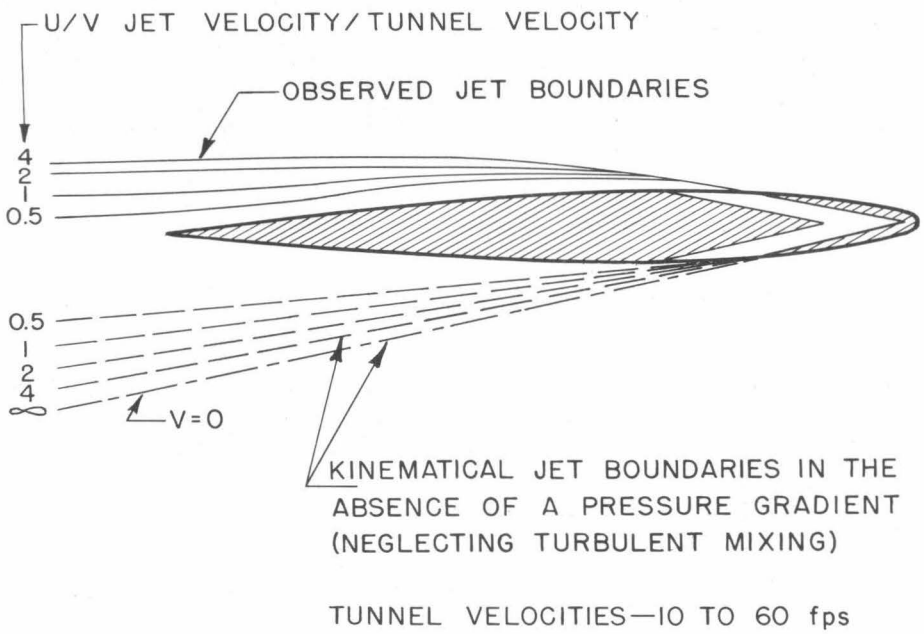

Fig. 14 - The effect of the velocity and pressure fields around the hydrofoil on the jet flow pattern

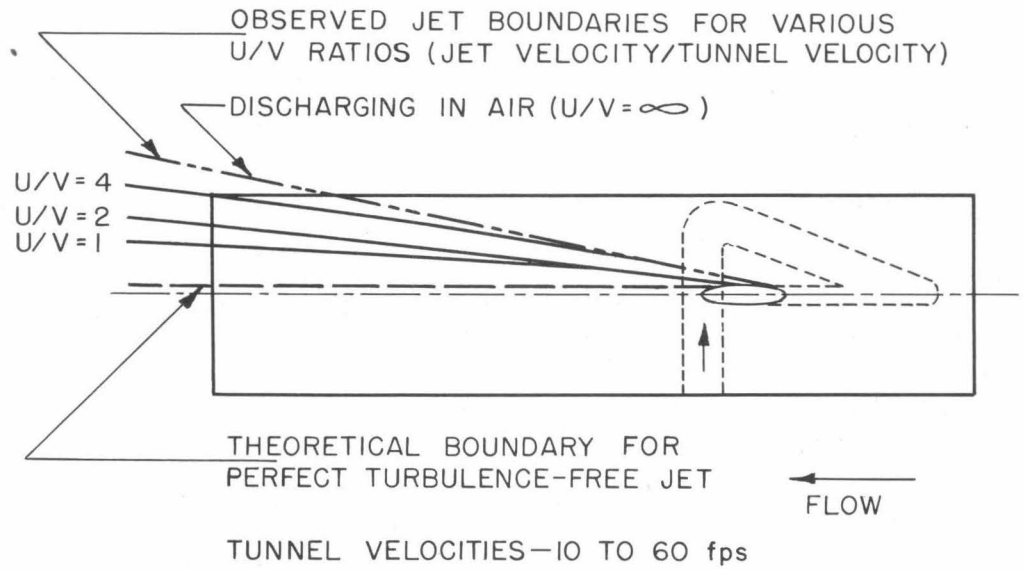

Fig. 15 - Observed jet boundaries under various flow conditions

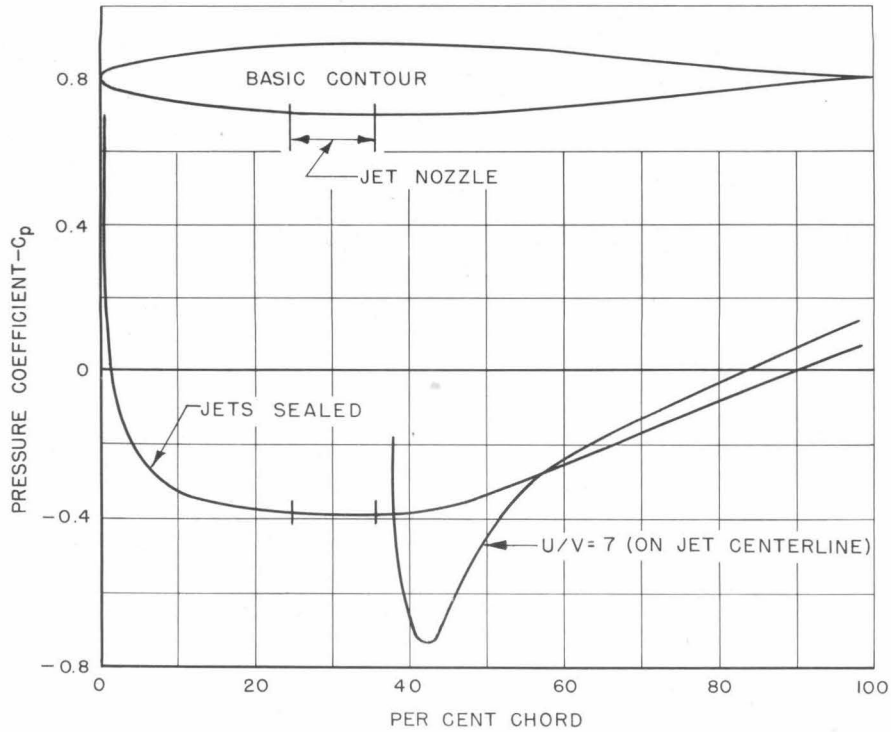

Fig. 16 - Pressure distribution around the NACA 63-010 hydrofoil

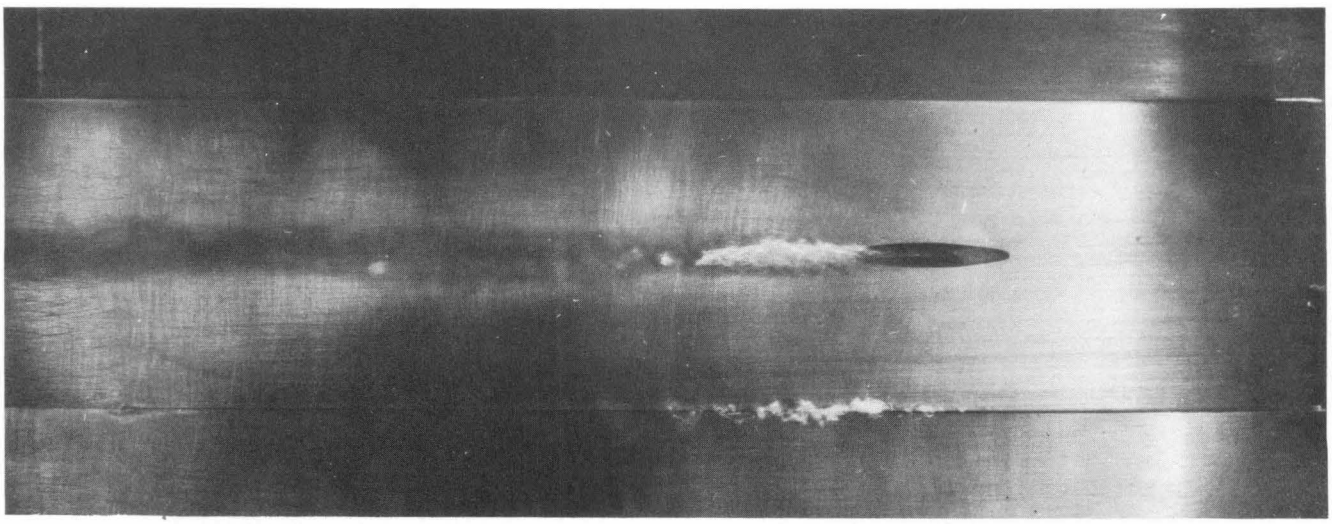

Fig. 17 - Cavitation in the low pressure region behind the jet nozzle. Tunnel velocity 90 fps; Jet velocity 90 fps.

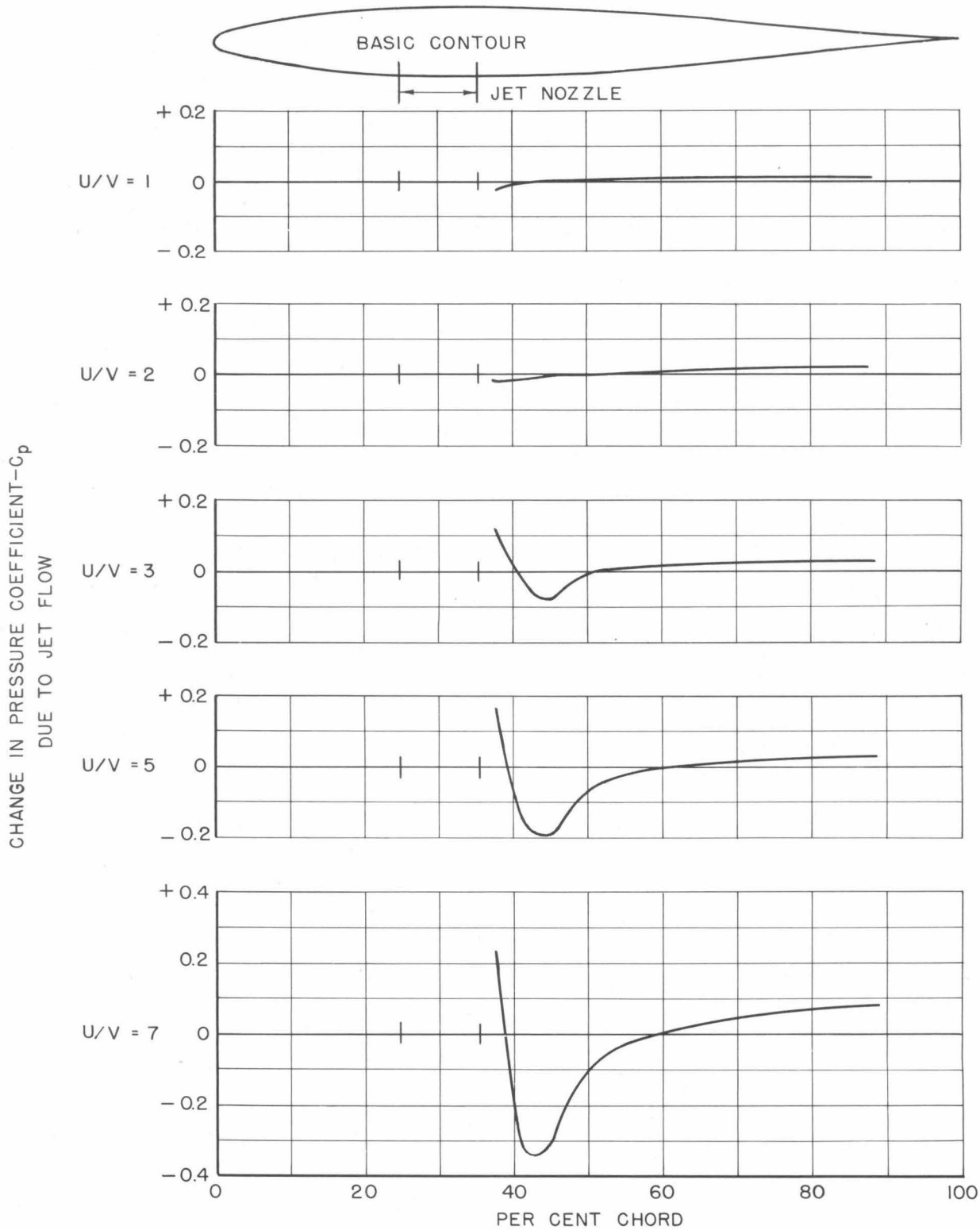

Fig. 18 - Change in pressure distribution along the axis of the jets for various jet-to-tunnel velocity ratios

Another indication of the changes in pressure distribution caused by the jet is shown by the family of pressure coefficient profiles on Fig. 19. This graph shows the spanwise change in pressure coefficient at various chord positions downstream from the jet for a jet velocity of 70 fps and a tunnel velocity of 10 fps. The jet extension as shown on this figure is about 9 jet diameters spanwise, while the measured model is 13 diameters wide.

Evidently percentage change of the drag coefficient is dependent on the span of the model – the measured change being all in the span covered by the jet extension, about 9 diameters in this case.

The nature of the pressure distribution is of interest in determining cavitation characteristics. However, additional information as to the pressure disturbances due to the jets can be obtained from the photographs in Figs. 20 and 21. In both cases the tunnel velocities are the same, v = 40 fps and the cavitation parameter K = 0.37. For the case shown in Fig. 20 for zero jet velocity, a fringe of cavitation exists along the surface of the hydrofoil. Notice the effect of the pressure difference due to hydrostatic head of 2-in. With the jet in operation at 80 fps, Fig. 21, the increase in surface pressure can be observed by the greatly reduced amount of cavitation on the model surface in the region above and below the jet. This indicates that the interference of the jets extends outside the area of the jet itself. The surface pressure downstream from the nozzle exit cannot be observed directly because the cavitation within the jet accentuated by the lowered pressure beyond the orifice along the nozzle axis extends into the stream and obscures the model surface.

It is important to notice that cavitation within the jets on the model does not indicate that cavitation must occur with the same combination of jet and tunnel velocity on another model or prototype. This cavitation is indicative only of the pressure and velocity conditions existing in the highly turbulent jet of the model that is quite different from the accelerated orderly flow with preceding straightening vanes, which is characteristic of the Mk 40 torpedo. The investigation of the effects of cavitation was not pursued beyond the preliminary stage.

There is need for more work with another model built for cavitation and pressure distribution runs only, and not mounted on the balance. Such a model equipped with properly contoured jets should be capable of reaching higher jet velocity ratios at higher tunnel speeds and have better jet cavitation

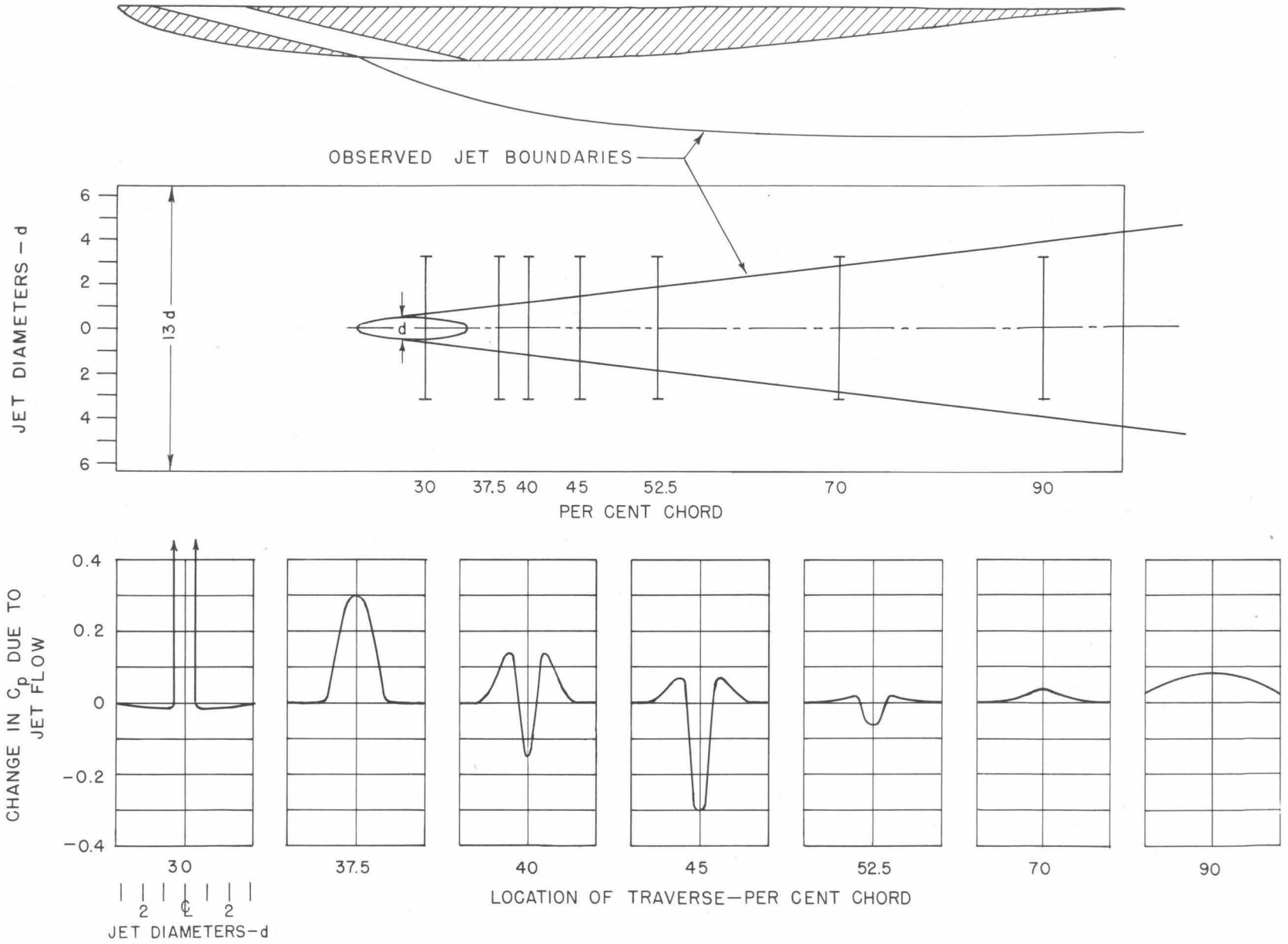

Fig. 19 - Spanwise change in pressure coefficient at several stations in the wake of the jets at a jet-to-tunnel velocity ratio of 7. V = 10 fps; U = 70 fps.

CONFIDENTIAL

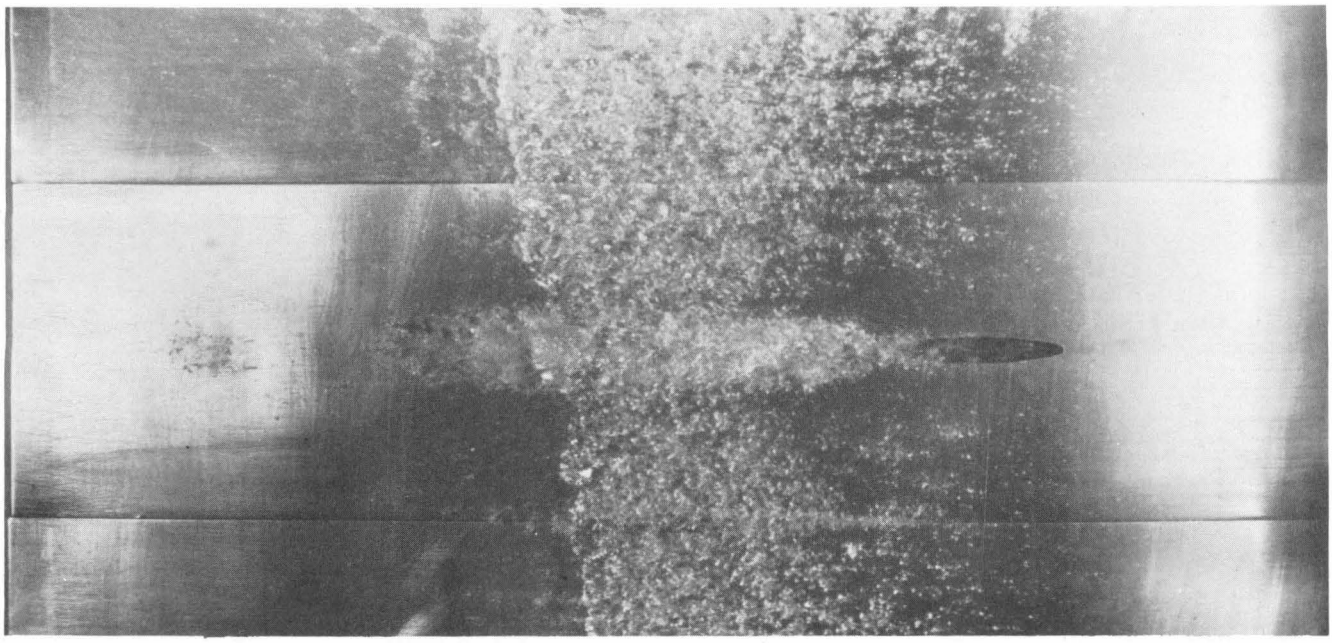

Fig. 20 - Effect of jets on cavitation of hydrofoil
Tunnel velocity = 40 fps; Jet velocity = 0 fps; K of model = 0.37

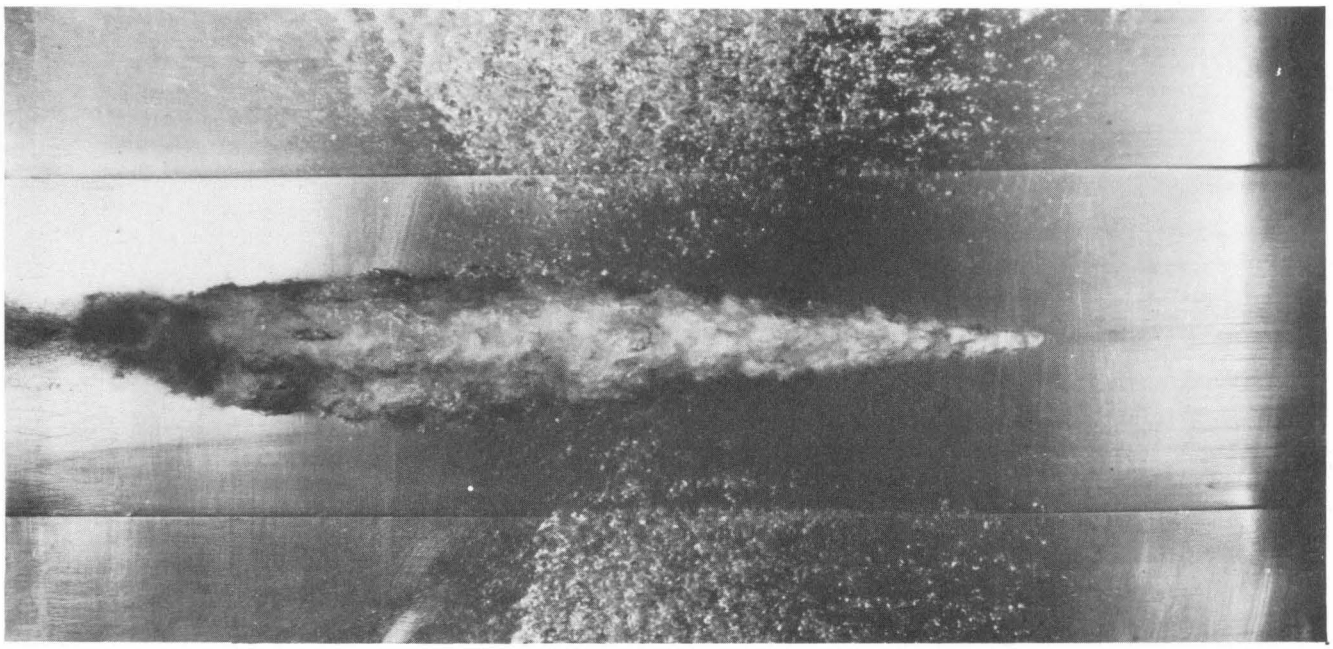

Fig. 21 - Effect of jets on cavitation of hydrofoil
Tunnel velocity = 40 fps; Jet velocity = 80 fps; K of model = 0.37

characteristics. In addition, further pressure distribution work should be done to investigate the pressure drag across the region of transition from reduced to increased drag.

APPENDIX

A. Trip Wire

Preliminary drag runs, using the force section with the jet nozzles sealed, produced data which showed scatter of the same magnitude as the effects to be investigated, particularly at lower velocities. In addition, the curves of drag coefficients turned rather sharply upward at higher Reynolds numbers, above 2.7×10^6. These runs seemed to indicate that the model was operating in the transition zone between laminar and turbulent boundary layer flow. Common practice at this and other laboratories for three-dimensional bodies has been to attach spoilers to the surface of the models to insure stable boundary layer conditions. However, this method has the disadvantage that the configuration of the model itself is changed. Following the method used in towing tanks, a thin trip wire was supported ahead of the model from the upper and lower shields. In a first attempt, a 13-in. span was used; however, this was changed to 4 in. to reduce the forces on the wire and the sag. Both stainless steel and piano wire from 0.005 to 0.025 in. diam. were tested, but in every case at velocities of less than 40 fps the wires failed in fatigue at the supports due to vibration. Nylon (0.013 to 0.025 in. diam.) and linen fishing leader was used at velocities up to 90 fps without breaking; however, its elasticity caused it to sag and change the distance ahead of the leading edge with velocity.

Finally, a 0.015 in. diam., seven-strand, twisted bronze wire fishing leader was found to work very satisfactorily and was used for the remainder of the tests. The trip wire installation can be seen in Figs. 7 and 22.

The position of the trip wire was varied from 0 to 1-7/8 in. ahead of the leading edge of the model. Fig. 23 shows that this model is insensitive to the distance behind the trip wire in the range from 1-7/8 to 1/8 in. As was expected when the trip wire was fastened directly to the model nose, the drag coefficient curve is only slightly different from that with no trip wire. Runs made at 20 fps and 60 fps with trip wire showed the pressure distribution to be independent of Reynolds number. Runs made with and without the trip wire

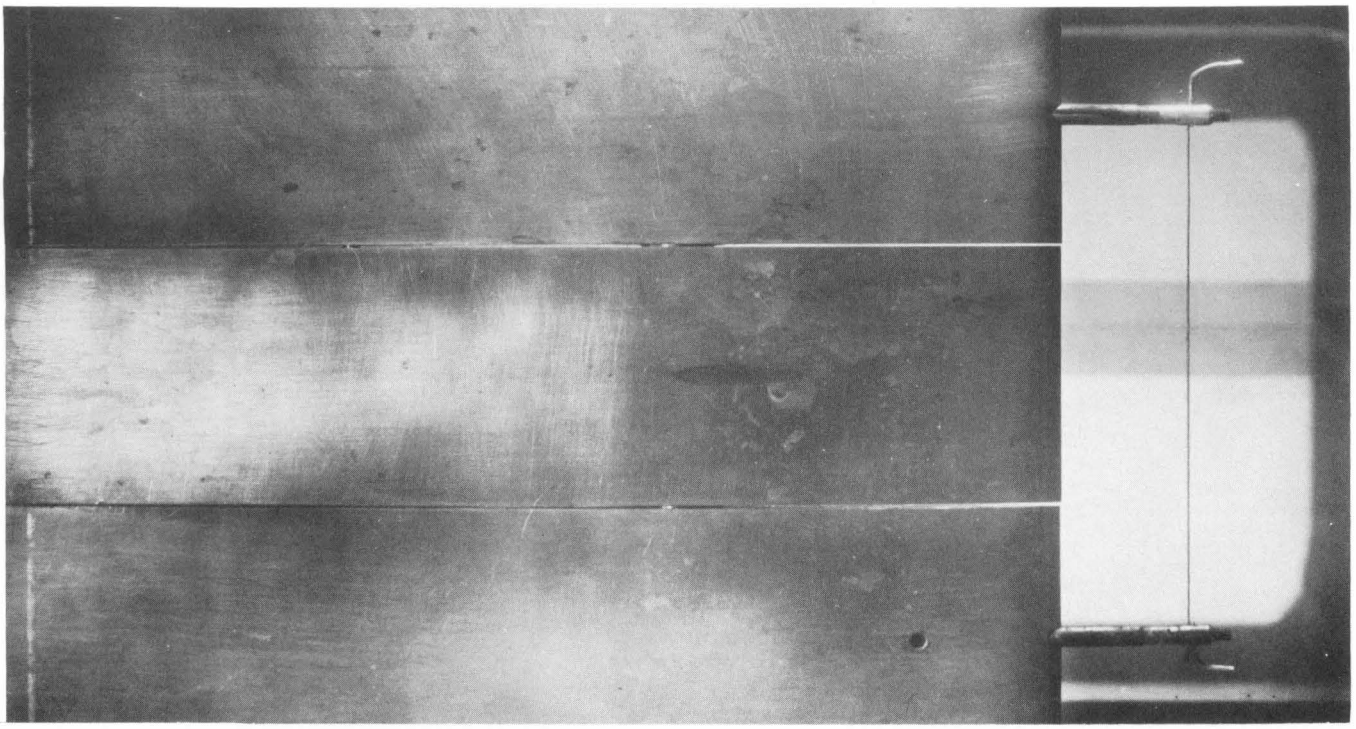

Fig. 22 - Force section with 0.015 in. dia. trip wire attached 7/8 in. ahead of model

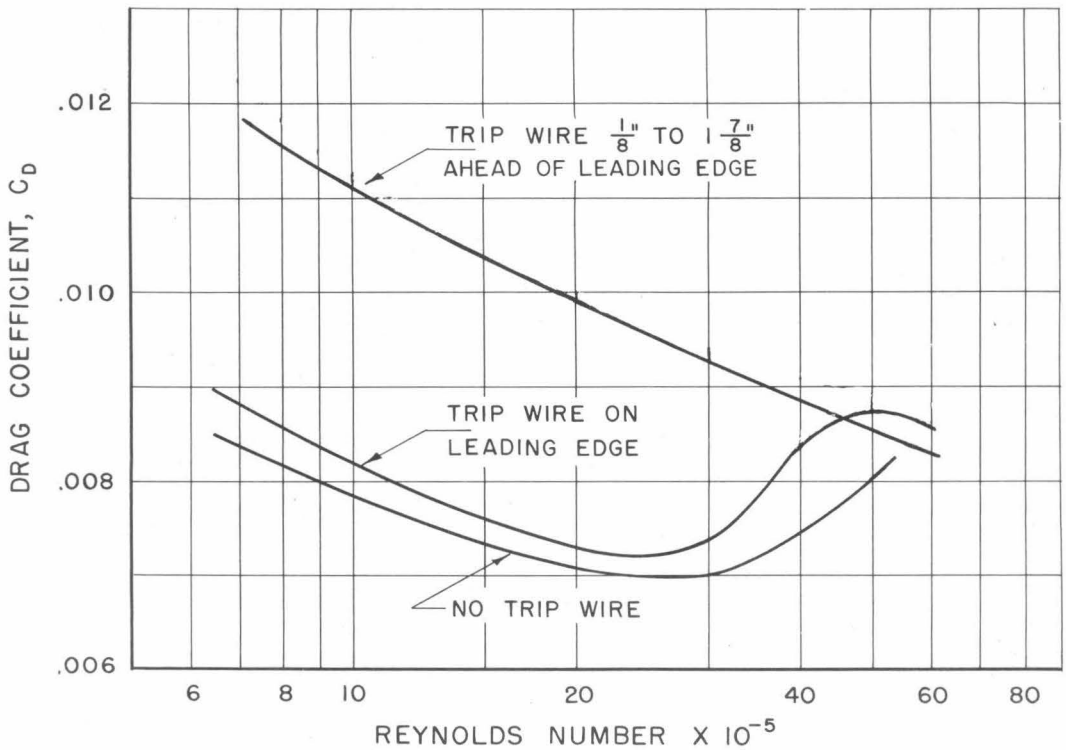

Fig. 23 - Effect of trip wire on the drag coefficient of NACA 63-010 hydrofoil without jets

at 20 fps gave the same results. However, runs at 60 fps showed a more efficient pressure recovery with the trip wire, Fig. 24. The trip wire, mounted approximately 5/8 in. ahead of the model, was used on all subsequent drag and pressure distribution runs.

B. Shield Gap Effect and Spindle Drag

The 2-in. span force section was mounted between but not touching the 6-in. span upper and lower shields. To approach two-dimensional flow as closely as possible, it was necessary to reduce the distance between the force section and the shields to a minimum without causing interference due to spindle deflection or pressure changes. In an attempt to calibrate this shield gap effect, smooth body drag runs were made with various upper gaps from 0.010 to 0.088 in. The results show the gap to have no measurable effect up to a width of approximately 0.030 in. at stream velocities less than 65 fps, as shown in Fig. 25. With the 0.088-in. gap, there is a marked increase in drag at velocities above 50 fps. However, as shown by the corrected curve, this increase at high velocities can be directly attributed to the increased drag on the spindle supporting the model.

Tests were made to measure the drag due to the water impinging on the portion of the spindle between the shields and the force section, Fig. 26. In these tests, the force section was removed and the drag on the spindle in the gap between the upper and lower shields was measured directly, as shown in the sketch, Fig. 27.

These two tests seem to show that forces on the spindle due to the gap between sections of the hydrofoil are negligible. The remainder of the tests were conducted with upper and lower gaps of approximately 0.010 in.; hence no correction for spindle drag or shield gap was needed.

C. Jet Thrust Calibration

The thrust of the jets was determined by calibration before any combined thrust and drag runs were attempted. The same setup was used as in the combined thrust and drag runs. Incorporated in the tunnel balance system is a 25-lb. drag and cross-force preload which permits negative force measurements of this magnitude. The preload system consists of a spring and lever arrangement which gives a constant preload despite small movements of the spindle. Fig. 28 shows four curves for comparison, two theoretical thrus

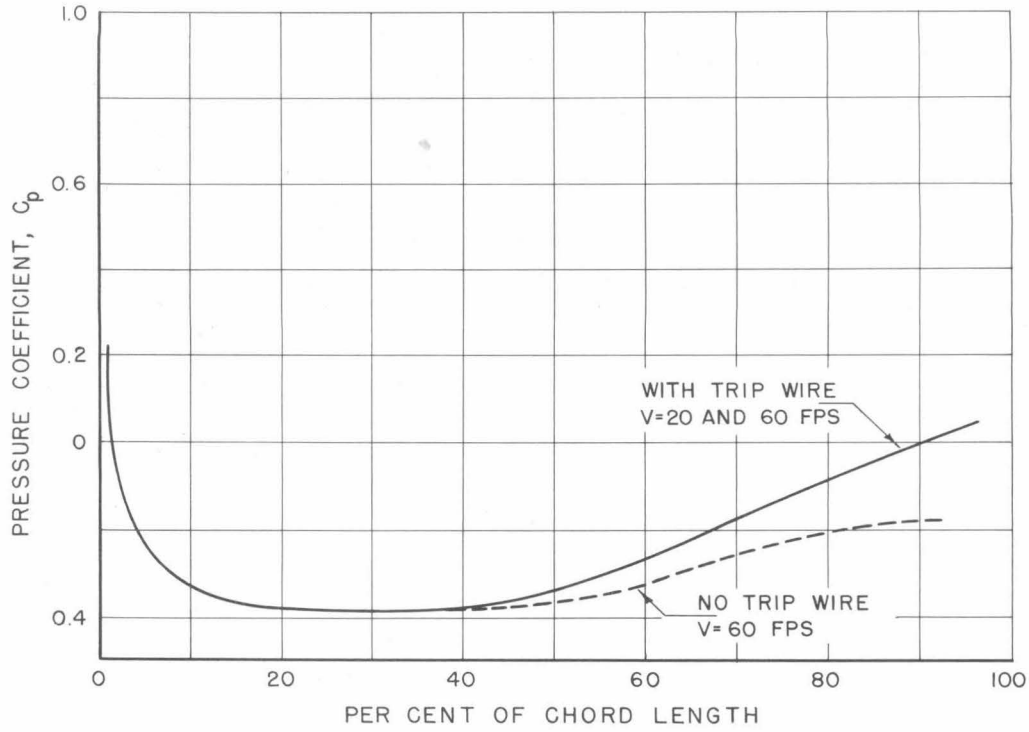

Fig. 24 - Effect of trip wire on the pressure coefficient of NACA 63-010 hydrofoil without jets

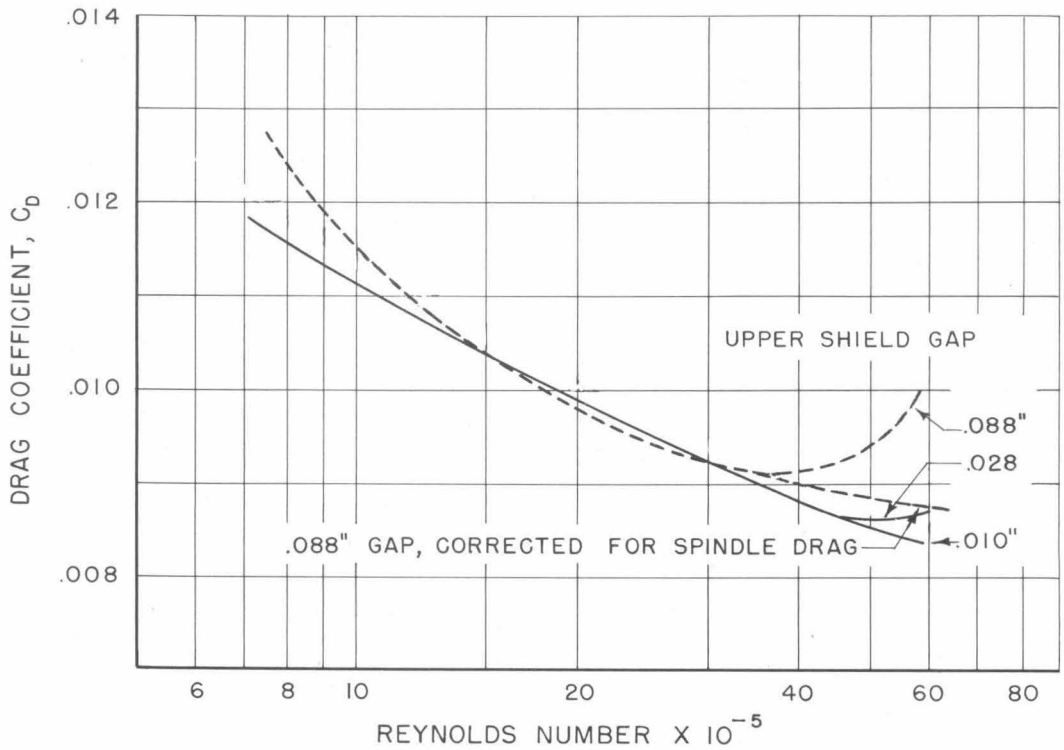

Fig. 25 - Effect of shield gap on the drag coefficient of NACA 63-010 hydrofoil without jets

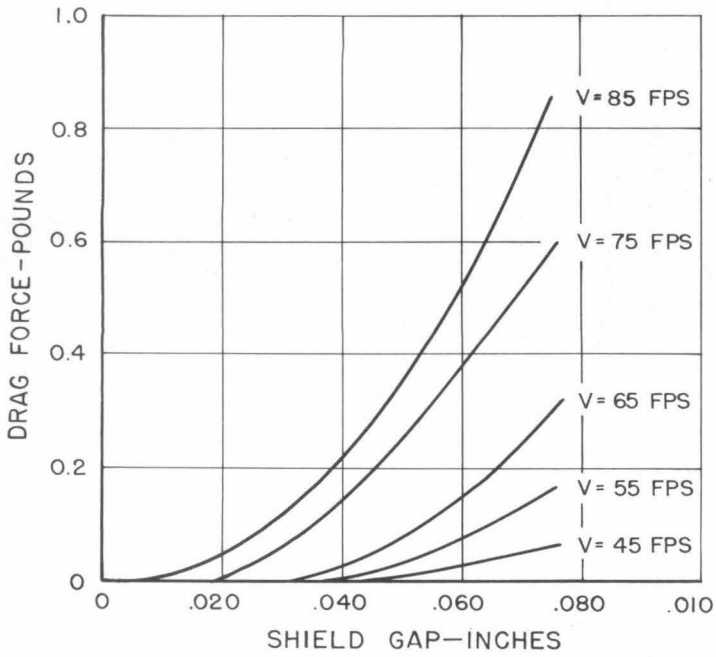

Fig. 26 - Drag on spindle vs. shield gap at various tunnel velocities

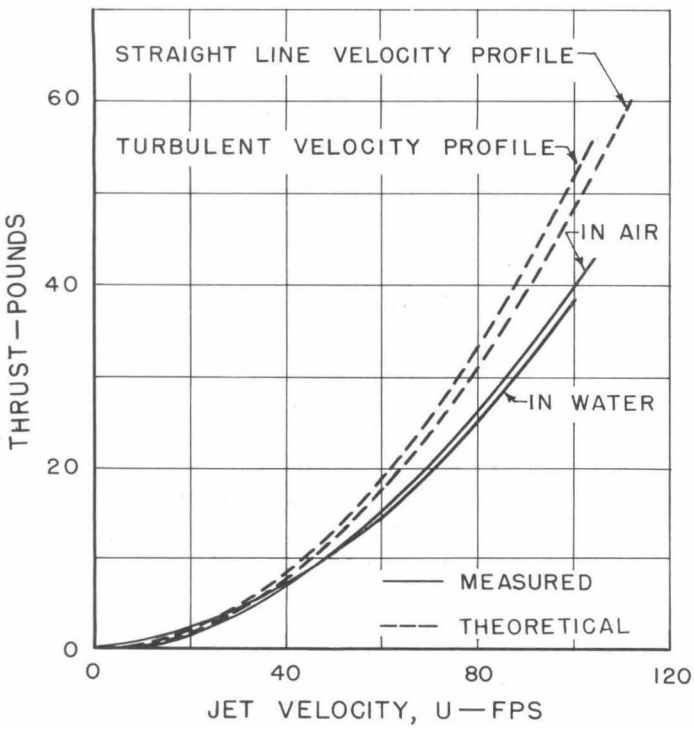

Fig. 28 - Measured and calculated thrust of hydrojets

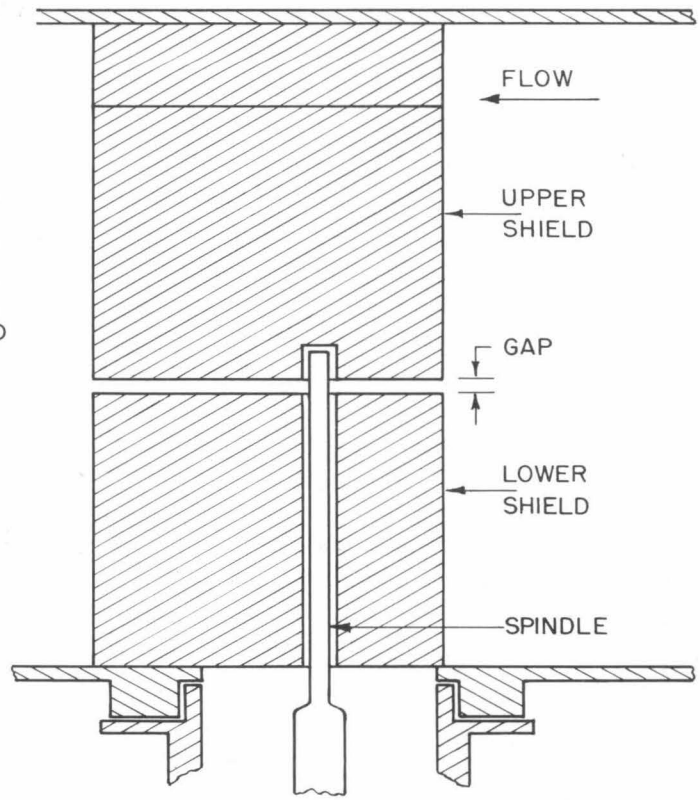

Fig. 27 - Setup for calibrating spindle drag

curves, as calculated by assuming (a) uniform jet velocity profile and (b) turbulent flow velocity distribution, and two measured thrust curves, one in air and one in water. The measured thrust curves are for a working section pressure of 80 psig. This pressure was sufficient to suppress jet cavitation even at the highest jet velocities.

It is interesting to note that with zero tunnel velocity and jet velocities less than 40 fps the thrust of the jets was greater with the model submerged than with the model in air. At jet velocities higher than 40 fps the thrust with submerged model was less than with the model in air. This increase in thrus or decrease in drag at low jet velocities and zero tunnel velocity is the same trend observed in the drag runs. At higher jet velocities the action of the jets and the induced flow around the hydrofoil reduced the measured thrust or increased the drag. Since this was one of the effects to be investigated, the thrust runs made in air were used in all the drag calculations.

D. Effect of Pressure on Thrust and Drag

The drag runs were made at constant tunnel pressure for all velocities. This resulted in lower jet nozzle outlet pressures at higher tunnel velocities. As a result of the low local pressures, the jets were observed to cavitate in the nozzles and a cloud of small bubbles appeared at high jet and stream velocities. In order to study this effect and to calibrate for the thrust at all jet exit pressures, a complete set of thrust runs was made with the working section filled with air at pressures of from –2 psig to 80 psig, Fig. 29. The marked increase in thrust at the lower pressures can be attributed to the fact that the jet velocity is increased due to the presence of air and vapor bubbles during cavitation. This effect is apparent in the total drag and thrust curves, which show a decrease in drag (Fig. 30); or an increase in thrust under conditions of velocity and pressure which caused the jets to cavitate.

At 100 fps jet velocity, determined by the measured rate of flow through the pump, divided by the jet outlet area, the thrust increased from 4.0 lb at 80 psig working section pressure to 6.15 lb at zero psig. This increased thrust represents a velocity increase to 128 fps at the low pressure.

This seeming gain in thrust is obtained by an increase in power input because the head (or pressure difference) has to be increased to produce the higher velocity. For the same pressure input, the flow velocity and thrust for a cavitating jet are lower than for a noncavitating jet.

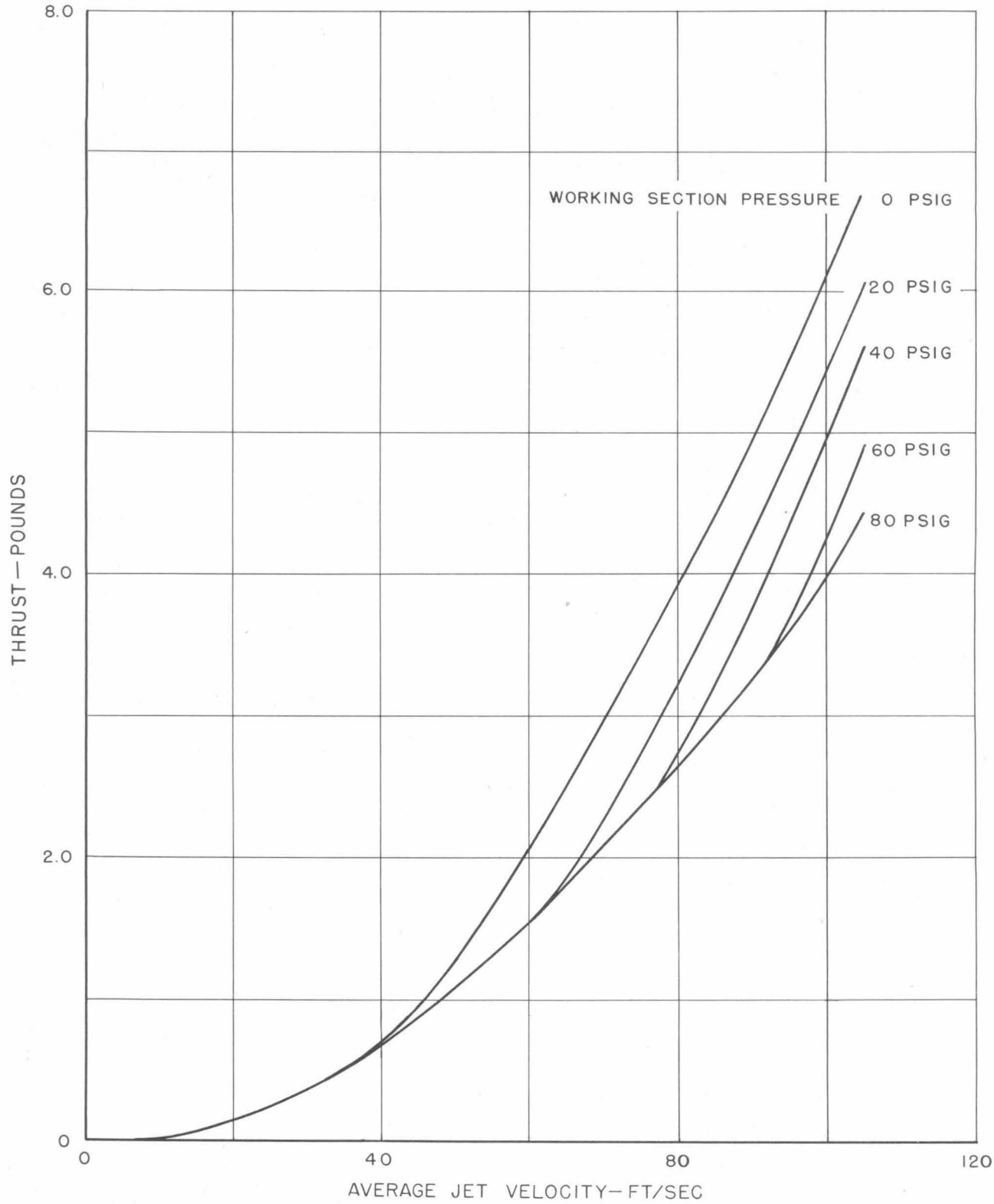

Fig. 29 - The effect of working section pressure on the thrust of the NACA 63-010 hydrojets discharging into air

In an attempt to eliminate the effect of jet cavitation from the results, the pressure at the jet nozzles was calculated for all tunnel velocities from the pressure coefficients as measured for the smooth hydrofoil. The thrust curve corresponding to this jet exit pressure was then used in conjunction with the measured combined drag and thrust curve to calculate the drag on the hydrofoil.

Keeping working section pressure at 20 psig, there is evidence of jet cavitation at jet velocity U = 65 fps and tunnel velocity V = 10 fps, and similarly for U = 40 fps and V = 80 fps. It was believed that cavitation in the jets could have some effect other than an increase in thrust; hence additional runs were made with a working section pressure of 70 psig. At this pressure the maximum attainable working section velocity is approximately 60 fps. At 80 fps the maximum working section pressure attainable with our equipment is 40 psig.

The runs made at these higher pressures gave results similar to those in which there was jet cavitation. Fig. 31 shows the effect of pressure on the combined drag and thrust at a tunnel velocity of 30 fps. The effect of the jet cavitation is to cause increase in drag at higher jet velocities, Fig. 32. This increase in drag is much less at higher stream velocities. Jet cavitation should be further investigated with a model having contoured jet nozzles.

E. Estimate of Accuracy of Data

The force indicating gages of the balance system of the High Speed Water Tunnel indicate force magnitudes to the nearest hundredth (0.01) of a pound. Calibration of the drag gage showed that the maximum error in the range from 0 to 75 lbs. was less than one-half of one percent (0.5%).

For the model without jets the sources of scatter in the data were two: small variations in tunnel velocity under supposedly constant conditions, and a fluctuating boundary layer transition point resulting from turbulence in the stream. The effect of small fluctuations in tunnel velocity was minimized by taking the average of a group of ten force gage readings taken at random intervals. Steady boundary layer conditions were approached by using a trip wire (see appendix, p.27). For the body with jets there were the additional factors of pump vibration and varying vertical loads and pressures on the spindle.

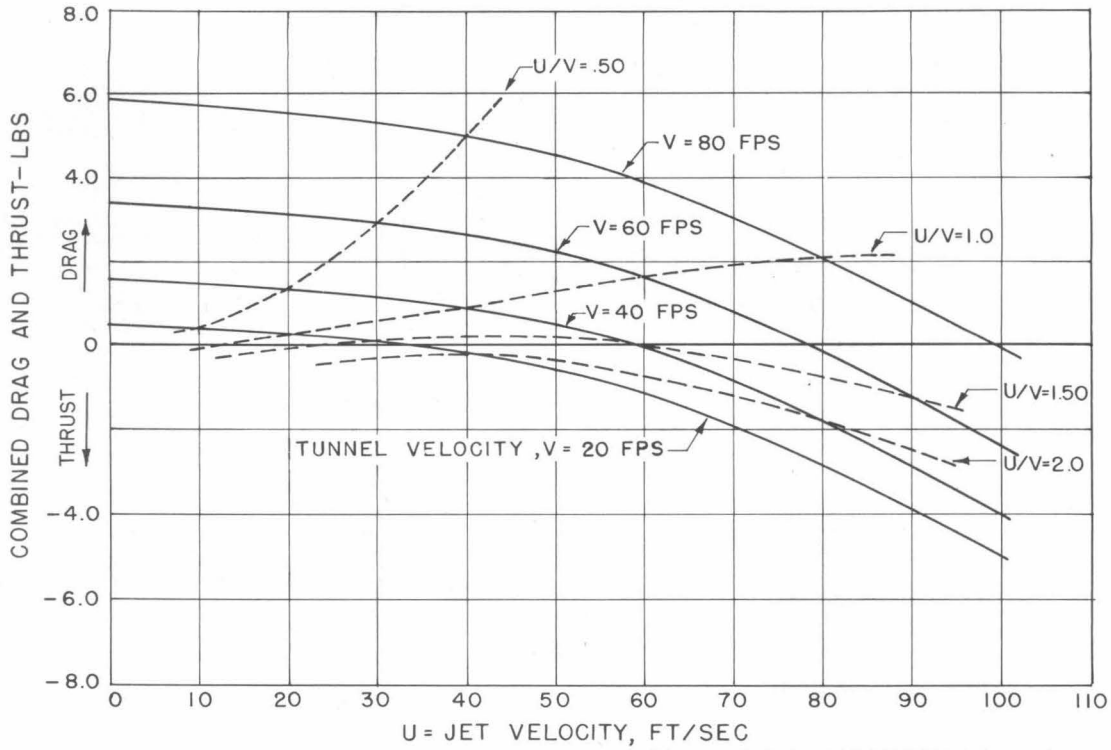

Fig. 30 - Measured combined drag and thrust vs. jet velocity for a series of tunnel velocities at a working section pressure of 20 psig

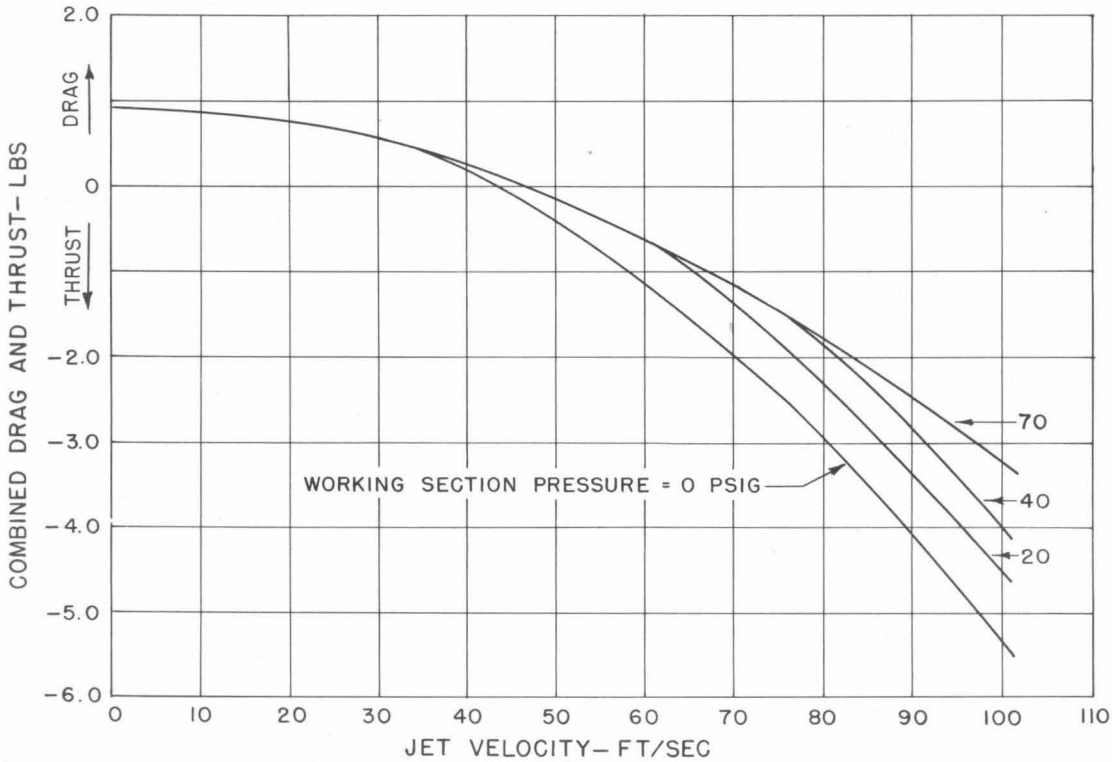

Fig. 31 - The effect of working section pressure on the measured combined drag and thrust at a constant tunnel velocity of 30 fps

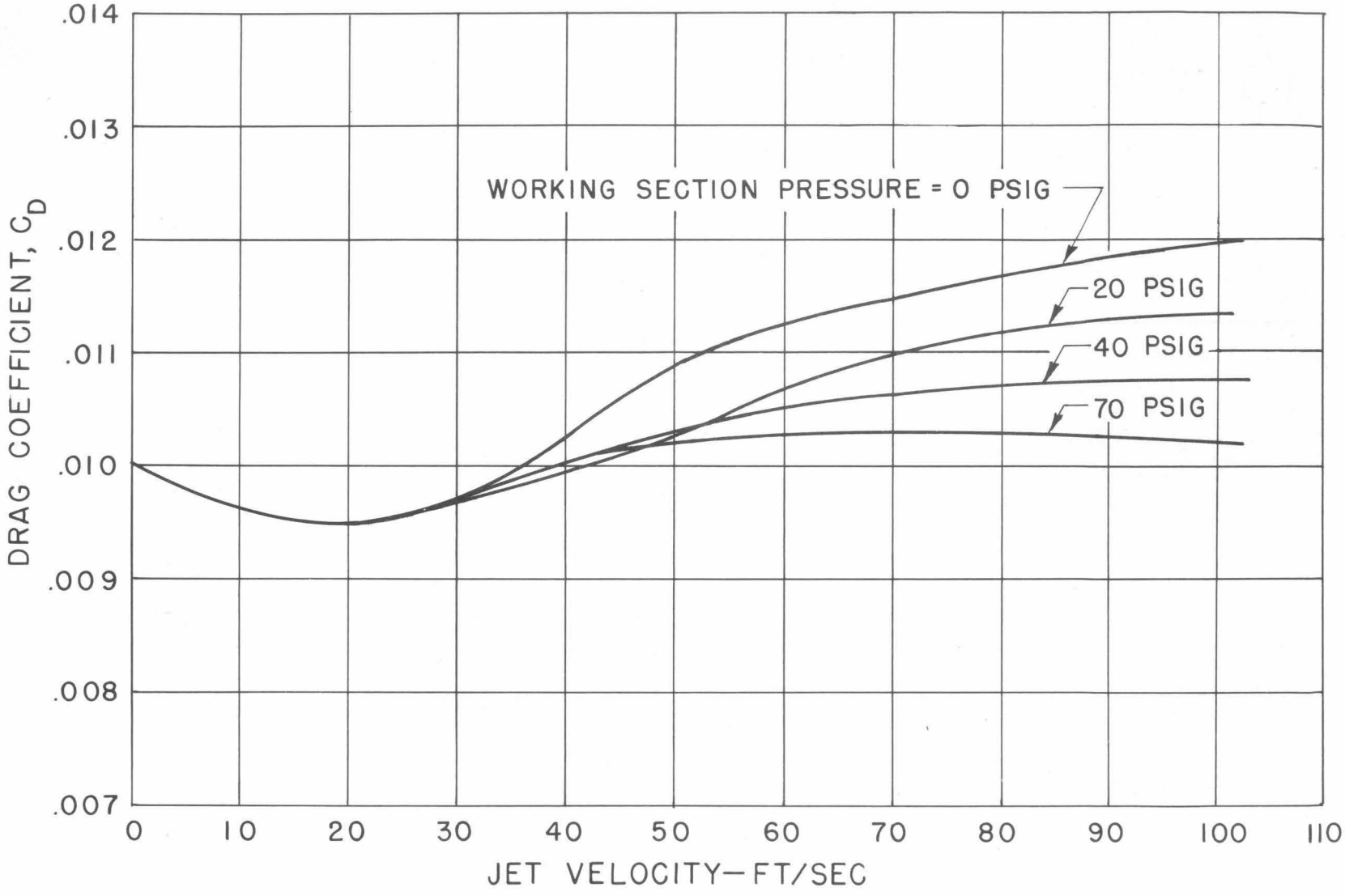

Fig. 32 - The effect of working section pressure on the drag coefficient at a constant tunnel velocity of 30 fps

In spite of precautions, considerable scatter in the data was observed for velocities of 20 fps and less. This scatter is difficult to avoid when studying slender bodies with good hydrodynamic characteristics and low drag coefficients. At 20 fps the maximum scatter was approximately 10 per cent. At 30 fps the maximum scatter was less than 5 percent, and at 40 fps and above, the maximum scatter was less than 2 percent.